









RESEARCH ARTICLE

10.1029/2020JD034332

Upper Troposphere Smoke Injection From Large Areal Fires

Stephanie Redfern^{1,2} , Julie K. Lundquist^{1,2} , Owen B. Toon^{1,3} ,
Domingo Muñoz-Esparza⁴ , Charles G. Bardeen^{1,4} , and Branko Kosović⁴ 

Key Points:

- Local atmospheric conditions affect plume lofting above large areal fires simulated by Weather Research and Forecasting (WRF-Fire) model
- Moisture has the largest impact on the amount of smoke lofted into the upper troposphere and lower stratosphere
- Faster wind speeds reduce the altitude of smoke lofting

Correspondence to:

S. Redfern,
stephanie.redfern@colorado.edu

Citation:

Redfern, S., Lundquist, J. K., Toon, O. B., Muñoz-Esparza, D., Bardeen, C. G., & Kosović, B. (2021). Upper troposphere smoke injection from large areal fires. *Journal of Geophysical Research: Atmospheres*, 126, e2020JD034332. <https://doi.org/10.1029/2020JD034332>

Received 6 DEC 2020
Accepted 8 NOV 2021

¹Department of Atmospheric and Oceanic Sciences, University of Colorado, Boulder, CO, USA, ²National Renewable Energy Laboratory, Golden, CO, USA, ³Laboratory for Atmospheric and Space Physics, Boulder, CO, USA, ⁴National Center for Atmospheric Research, Boulder, CO, USA

Abstract Large areal fires, such as those ignited following a nuclear detonation, can inject smoke into the upper troposphere and lower stratosphere. Detailed fire simulations allow for assessment of how local weather interacts with these fires and affects smoke lofting. In this study, we employ the fire simulation package in the Weather Research and Forecasting (WRF-Fire) model, Version 4.0.1, to explore how smoke lofting from a fire burning a homogeneous fuel bed changes with varying local winds, relative humidity, and atmospheric boundary-layer stability for two different-sized areal fires. The presence of moisture has the greatest influence on the results by raising the altitude of lofting, while faster wind speeds dampen lofting and lower the injection height. Stably stratified conditions inhibit plume propagation compared with neutrally stratified conditions, although the impact of stability is not as strong as that of moisture and winds. These findings highlight the importance of using an appropriate atmospheric profile when simulating large fires, as the local weather can have a meaningful influence on smoke lofting.

1. Introduction

Large fires have the potential to loft considerable amounts of smoke high in the atmosphere. If the fires burn intensely enough, their sensible heat flux can generate powerful convection (Luderer et al., 2006; Trentmann et al., 2006). Convection can also be enhanced by cloud formation if the atmosphere is humid. Aerosol byproducts of combustion can act as cloud condensation nuclei (CCNs), which can seed pyrocumulus (fire-derived clouds, or pyroCu) and pyrocumulonimbus (fire-derived storms or pyroCb) development. A pyroCb forms from deep convection, which has the potential to inject smoke into the upper troposphere and lower stratosphere (UTLS). When aerosols rise to the UTLS, high-speed, upper-level winds can advect them to locations far from the fire source before they are removed from the atmosphere, and therefore they can affect climate elsewhere over months or years (Fromm et al., 2010; Peterson et al., 2014, 2018; Yu et al., 2019).

The impact of smoke in the UTLS on climate has been a research topic for decades. In particular, before the relatively recent intensification of wildfires due to climate change (Barbero et al., 2015; Boer et al., 2020; Gillett et al., 2004; Goss et al., 2020; Krikken et al., 2019; Westerling et al., 2011), research in this area was motivated by concerns of nuclear conflict during the Cold War era. Tensions at this time between the United States and the Soviet Union, who collectively possessed 70,000 nuclear weapons, posed the risk of nuclear war (Toon et al., 2008). This number of nuclear warheads far exceeded the numbers of military targets, so urban areas were almost certain to be targeted. Nuclear weapon attacks on these dense fuel beds could light powerful fires that would burn for days, sending large amounts of aerosols very high in the atmosphere. Concern over how this UTLS smoke would impact regional and global climate, motivated by what was observed during firestorms that had occurred in Hiroshima after the first nuclear attack in World War II and in Hamburg during that same time, prompted various studies evaluating such an event.

The majority of research on atmospheric impacts from nuclear war suggested grim impacts. In an early research study, Crutzen and Birks (1982) suggested that urban attacks might cause fires in surrounding forested regions, leading to very dense but short-lived smoke palls (Crutzen & Birks, 1982). Another early study, Turco et al. (1983), found that whole cities—with much larger fuel loads than forests—could be ignited, with powerful enough convection to loft combustion byproducts into the upper troposphere and stratosphere, where residence times could be on the order of years (Turco et al., 1983). In a few weeks' time, these aerosols would circle the planet and limit sunlight globally. As a result, following significant drops in temperature and ensuing crop failure, people would fall victim to freezing temperatures and food shortages. This outcome was given a name: nuclear

© 2021. The Authors.

This is an open access article under the terms of the [Creative Commons Attribution-NonCommercial-NoDerivs License](https://creativecommons.org/licenses/by-nc-nd/4.0/), which permits use and distribution in any medium, provided the original work is properly cited, the use is non-commercial and no modifications or adaptations are made.

winter (Turco et al., 1983). Ultimately, collective scientific evidence of nuclear winter potential led leaders of the United States and Soviet Union to begin the process of denuclearization.

Despite denuclearization efforts over the last 40 years, however, nine nations still possess a total of 14,000 nuclear weapons, of which about 5,000 are deployed (with the rest being dismantled) (SIPRI, 2019). This stockpile is enough to attack with more than ten weapons each city with over 100,000 people in the U.S., Russia, and China (Arms Control Association, 2019; Kristensen, 2019). Nuclear winter, therefore, remains a risk, and studies on the phenomenon using more modern modeling methods continue.

Recent research on atmospheric effects of nuclear conflicts has employed both global climate models (GCMs) and high-resolution models, generally corroborating the findings of early studies (Cotton, 1985; Coupe et al., 2019; Covey et al., 1984; Ghan et al., 1988; Penner et al., 1986; Reisner et al., 2018; Robock, Oman, & Stenchikov, 2007; Robock, Oman, Stenchikov, et al., 2007; Robock & Toon, 2012; Toon et al., 2007; Wagman et al., 2020). Most GCM-based studies are initialized with a user-specified amount of smoke loading at a specified injection height, based on the scenario being considered. The injection heights are often informed by observations from mass fires, such as in Hamburg during WWII, or on 1,980s simulations using mesoscale models that were driven by energy release rates (Penner et al., 1986; Small & Heikes, 1988; Turco et al., 1990). Using this method, Coupe et al. (2019); Robock, Oman, Stenchikov, et al. (2007), Toon et al. (2007), and Toon et al. (2008) found that, given an exchange with the strategic weapons allowed under treaties between the U.S. and Russia, a nuclear winter is a possible outcome. Further, the detonation of 100 Hiroshima-sized bombs in Pakistani and Indian urban areas—another region with persistent bilateral tensions between two nuclear-armed nations—could produce climate effects that endanger global agricultural productivity (Jägermeyr et al., 2020; Toon et al., 2019; Xia et al., 2015). Only 1.5 megaton's worth of explosives used on urban areas could cool global average temperatures by 1.25°C for several years and cause anomalously cold temperatures of 0.5°C for over a decade (Toon et al., 2019).

In contrast to the above findings, Reisner et al. (2018) suggest that the risk of significant climate perturbations is small because the bulk of the smoke rising from urban targets will not ascend above the lower troposphere. This particular study used a fine-resolution model, HIGRAD-FIRETEC (FIRETEC), to simulate a detonation in the East Lake country club region of Atlanta (Robock, Toon, & Bardeen, 2019) to predict a smoke concentration profile, which was then incorporated into a global climate model to assess the impacts of high-altitude smoke transport following a broader-scale nuclear exchange. The selection of atmospheric parameters for the microscale model—namely the wind, thermal, and moisture profiles—are all defined in a manner to inhibit plume rise. Previous research focused on local smoke lofting, rather than on global climatic effects, has indicated that weather plays a significant role in fire plume behavior, which then affects how much smoke is injected in the UTLS. In particular, observational studies have noted that pyroCu and pyroCb development is sensitive to local environmental moisture (Fromm et al., 2010; Lareau & Clements, 2016; Luderer et al., 2006; Peterson, Hyer, et al., 2016; Sofiev et al., 2012; Trentmann et al., 2006), and as previously mentioned, these phenomena can inject aerosols into the UTLS.

Additionally, other studies have found that wind speeds determine whether or not a mass fire develops into a conflagration, which spreads quickly downwind, or a firestorm, which remains relatively stationary (Cotton, 1985; Glasstone & Dolan, 1977; Penner et al., 1986). Firestorms exhibit inward flow of near-surface air from every radial point toward its center and generate their own wind systems (Countryman, 1964; Morton, 1964). Firestorms are more likely to consume all the fuel in the ignition area and loft it to higher altitudes than conflagrations. Because Reisner et al. (2018) assumed a dry atmosphere and gusty boundary layer, their results may not have been wholly representative of nuclear winter risk. These omissions are important to address because the conclusion from that study suggests minimal climatological impacts from nuclear conflict. To address these concerns about the microscale modeling presented in Reisner et al. (2018), we have constructed a modeling study focused on the importance of how finer-resolution, idealized fire models are set up and how the atmospheric parameters may affect their predicted smoke profiles. Specifically, we assess the sensitivity of smoke lofting to local, background weather conditions.

In this study, we use large-eddy simulations (LESs) to simulate fire growth in a homogenous, heavy logging slash fuel bed to evaluate smoke lofting resulting from a mass fire, on time scales relevant to plume behavior. We quantify the sensitivity of this lofting to varying atmospheric conditions (horizontal wind speeds, background atmospheric humidity, and stability). Two fire sizes are considered, which are informed by the presumed affected

Table 1
WRF Configuration

WRF parameter	d01	d02
Horizontal resolution	1.1 km	100 m
Horizontal extent (Grid Cells)	200 × 200	199 × 199
Number of vertical levels		80
Model top		18 km
Lowest vertical level		60 m
Time step	3 s	0.27 s
Time integration scheme	Runge-Kutta 3rd order	
Advection scheme	5th-order horizontal; 3rd order vertical	
Coriolis parameter	10^{-4} s^{-1}	
Planetary boundary layer scheme	MYNN	-
Eddy coefficient option	2D horizontal diffusion	1.5-order SGS TKE
Surface layer scheme	MYNN	
Turbulence and mixing	-	Isotropic with 1.5-order TKE closure scheme
Damping	Upper-level Rayleigh layer of 0.33 s^{-1} with a depth of 5 km	
Roughness length	0.3 m	
Microphysics scheme	Thompson	
Boundary conditions	Periodic	Interpolated, One-way Nested
Fire grid mesh	-	4:1
Ignition radius	-	2 km or 4 km
Fuel source	-	Logging slash, 0.9 m depth (1.3 g cm^{-2}) or 0.3 m depth (0.26 g cm^{-2})
Smoke handling	-	Passive tracer

areas following a small-sized (15 kiloton) nuclear weapon air burst, which is consistent with the Hiroshima nuclear explosion, and a larger weapon (100 kiloton), which could be present in the Indian arsenal, since they exploded a weapon with a yield near 50 kt in 1998 (Wellerstein, 2012). The makeup of the fuel bed is less dense than what would typically be found in an urban setting due to model constraints, although it is still denser than the fuel makeup of Reisner et al. (2018). Fuel loading, at 1.3 g cm^{-2} , is an order of magnitude or more lower than what would be expected if the fire area consisted of buildings, refineries, and other similar targets. Consequently, this smoke sensitivity study primarily focuses on the relative importance of specific atmospheric phenomena on smoke rise. Longer-term radiatively driven lofting, which has been seen in observations (Yu et al., 2019) and represented in climate models (Coupe et al., 2019; Robock, Oman, Stenchikov, et al., 2007), is not considered.

The simulations and model setup are described in Section 2. In Section 3, we address the role of oxygen starvation, present our findings on how wind speeds, atmospheric moisture, and boundary-layer stability affect vertical smoke distributions, and compare several metrics to evaluate the comparative sensitivity of plume rise to environmental winds and humidity. Finally, we provide a brief discussion and conclusions in Section 4.

2. Model Environment

The simulations use the Advanced Research Weather Research and Forecasting Model (WRF-ARW, henceforth referred to as WRF), Version 4.0.1 (Powers et al., 2017; Skamarock et al., 2019). WRF is a numerical weather prediction model capable of simulating nested domains with outer boundaries specified either by coarser-scale models or reanalysis data, or by idealized conditions—the latter of which is useful for parameter sensitivity studies like this one. As an open-source model, WRF offers ease of accessibility and, therefore, simulation reproducibility. The model setup, explained below, is also summarized in Table 1.

WRF-Fire, the fire modeling parameterization in WRF, simulates the fire spread and heat release (latent and sensible) that results from a wildland fire. This heat release feeds back into the atmospheric component of WRF, influencing local meteorology. A passive smoke tracer option may be activated. WRF-Fire was first introduced in 2004 as an integration into WRF that coupled the CAWFE tracer model with a level-set fire spread algorithm (Clark et al., 2004; Coen et al., 2013; Mandel et al., 2011; Patton & Coen, 2004). In this study, we use a more recent version of WRF-Fire, in which a level-set method, which is a mathematical algorithm used to track front propagation (Osher & Sethian, 1988), is used to determine the fire spread. This technique improves the accuracy of its fire-front tracking by incorporating high-order numerical schemes and solutions of an additional equation for level-set re-initializations (Jiménez et al., 2018; Muñoz Esparza et al., 2018).

2.1. Model Setup

As described in Table 1, the simulations include two atmospheric domains: an outer mesoscale domain with periodic boundary conditions (referred to here as the parent), providing the reference flow, and a nested LES (referred to here as the nest). The outer domain has a horizontal grid resolution of 1.1 km across a 200×200 km domain. The nest is centered inside the parent, with a horizontal grid resolution of 100 m and spanning a 19.8×19.8 km domain. The vertical resolution for both domains is the same, with 80 levels stretched between the ground and the model top at 18 km. Due to the low model top, we assume a midlatitude location with a tropopause at 12 km and a Coriolis parameter of 10^{-4} s^{-1} (Wilcox et al., 2012).

Within the LES nest, a ground-level, 2D subgrid (referred to here as the fire mesh or just the mesh) spanning the floor of the entire nest is defined, and its sole use is to track the fire spread and fuel depletion per cell per time step. No atmospheric modeling occurs in the fire mesh. WRF utilizes a level-set algorithm within the mesh to more accurately track the fire front than otherwise would be possible using the coarser LES domain (Muñoz Esparza et al., 2018). The fire mesh resolution for these simulations is 25 m (that is, in this study, four fire mesh cells per LES grid cell). A depiction of a 1×1 km section of the nest with the fire mesh grid laid out on top of it is shown in Figure 1.

The fire is lit in the center of the nest, and atmospheric feedback from the nest to the parent does not occur. The simulations automatically terminate when the fire reaches the edge of the nest (as well as, by definition, the mesh), which could occur as quickly as 1.5 hr for the high wind speed simulations used in this study.

WRF physics and dynamics are simplified. The outer domain uses the Mellor-Yamada-Nakanishi-Niino (MYNN) planetary boundary layer (PBL, referred to later as the ABL) parameterization (Nakanishi & Niino, 2009). Since the nest is configured with LES resolution, no PBL scheme is required or specified. Both domains use Thompson graupel microphysics. This is a largely single-moment microphysics parameterization (cloud ice number concentrations are calculated) that does not incorporate aerosol interactions with cloud formation (Thompson et al., 2004, 2008). The MYNN surface-layer scheme is used to account for near-surface heating impacts, but no land-surface parameterization is used. For simulations incorporating radiative fluxes, the Rapid Radiation Transfer Model for the Korean Integrated Model (RRTMK) short- and longwave schemes is enabled (Baek, 2017). The model is initialized and run in a non-hydrostatic environment. A third-order Runge-Kutta time integration scheme is used, with a time step of 0.5 s in the outer domain. Eddy diffusion is handled by horizontal Smagorinsky first-order closure for the mesoscale domain, and by 1.5 order TKE closure for the LES nest. Moisture and scalar advection variables are calculated via a positive-definite scheme. Fifth-order horizontal and third-order vertical advection accuracy is used. To reduce the impact of gravity wave reflection within the domain, upper-level Rayleigh damping with a coefficient of 0.2 s^{-1} is employed within a depth of 5 km from the model top (Klemp et al., 2008). This damping layer is not expected to affect smoke lofting within the vertical range of interest in this study.

2.2. Simulations Overview

We vary geostrophic wind speed and wind shear, atmospheric moisture, boundary-layer stability, and ignition area in 20 different simulations to evaluate how meteorological variables influence the smoke distribution generated from two different-sized mass fires. The simulations are divided into groups defined by the input parameter being evaluated. In all cases, the outer domain is initialized and run (spun up) for four hours to achieve equilibrium from the initial condition, after which the interior domain is initialized and run for either 4 or 6 hr,

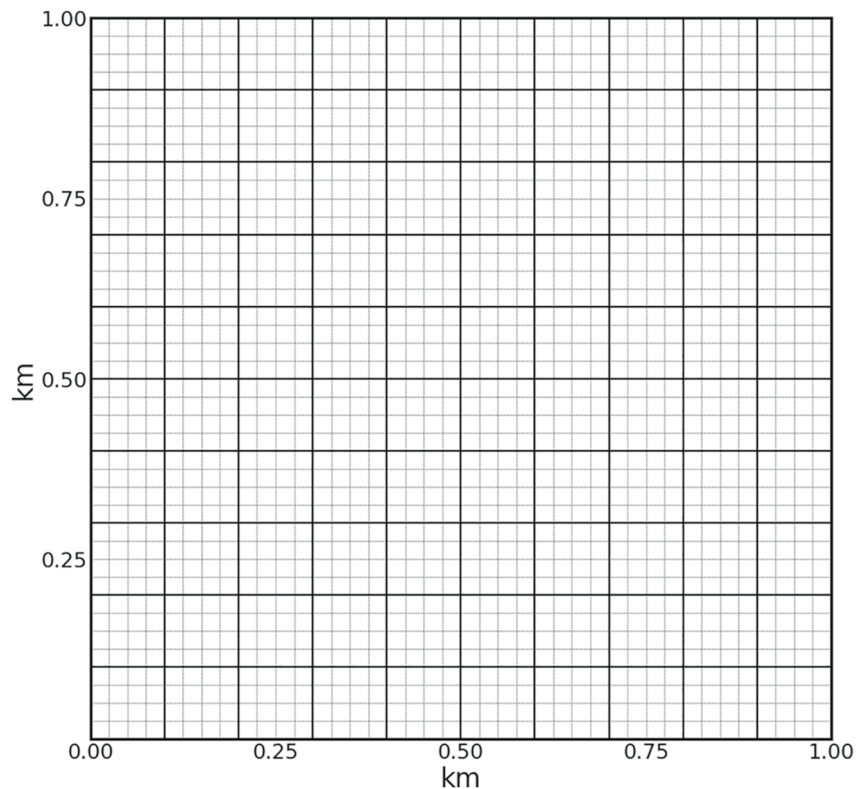


Figure 1. A 1×1 km section of the nest is shown, with the gridded fire mesh. The thick grid lines indicate the nest grid (100m resolution), while the thin grid lines show the mesh grid (25 m resolution).

depending on turbulence generation in the nested domain, before the fire is lit. The cell perturbation method (Muñoz-Esparza & Kosović, 2018) is used to generate TKE in the nest. Once the domains have been spun up, a fire is ignited in the center of the inner domain and burns for 90 min, with the exception of the high wind (HiWi) simulations, in which the fire intersects the domain boundary in less than an hour. Output from this final segment of the simulations is evaluated here.

Four different wind speed cases for each fire size are considered. The cases are forced by winds increasing from the ground up to a steady 2.5 m s^{-1} above the ABL (LoWi), to a steady 5 m s^{-1} above the ABL (MedWi), to a steady 10 m s^{-1} above the ABL (MiHiWi), and to a steady 15 m s^{-1} above the ABL (HiWi). These cases all have no radiation, a dry atmosphere, and a neutrally stratified, 2-km deep boundary layer capped by a stable layer ($\frac{\partial\theta}{\partial z} = 6 \text{ K km}^{-1}$) extending through the troposphere. At the tropopause, the transition to the stratosphere is defined by an even stronger inversion ($\frac{\partial\theta}{\partial z} = 15 \text{ K km}^{-1}$). These values have been selected based on the thermal profile used in the Reisner et al. (2018) study.

A base case for comparison against each of the other parameters is defined. This case is the low-wind scenario, with constant 2.5 m s^{-1} geostrophic winds defined throughout the domain (however, drag at the surface induces a nonlinear wind profile in the boundary layer during and after spinup). As with the wind speed cases, there is no radiation, a dry atmosphere, and a neutrally stratified, 2-km deep boundary layer capped by a stable layer extending through the troposphere (Figure 2). The thermal profile for this case has been defined as such to allow for a straightforward comparison with Reisner et al. (2018).

The other cases are divided into subsets based on variations in boundary-layer stability (Stable, with $\frac{\partial\theta}{\partial z} = 6 \text{ K km}^{-1}$ from the surface to the tropopause) and moisture and radiation (M50, MR25, MR50, MR75), which include predefined environmental relative humidities greater than zero. Specifications for each simulation can be found in Table 2. Each of these groups of cases are defined via the same atmospheric profile as the base case, except each group varies one (or in the case of moisture and radiation, two) of the input parameters (for example, the stable case has a stable ABL).

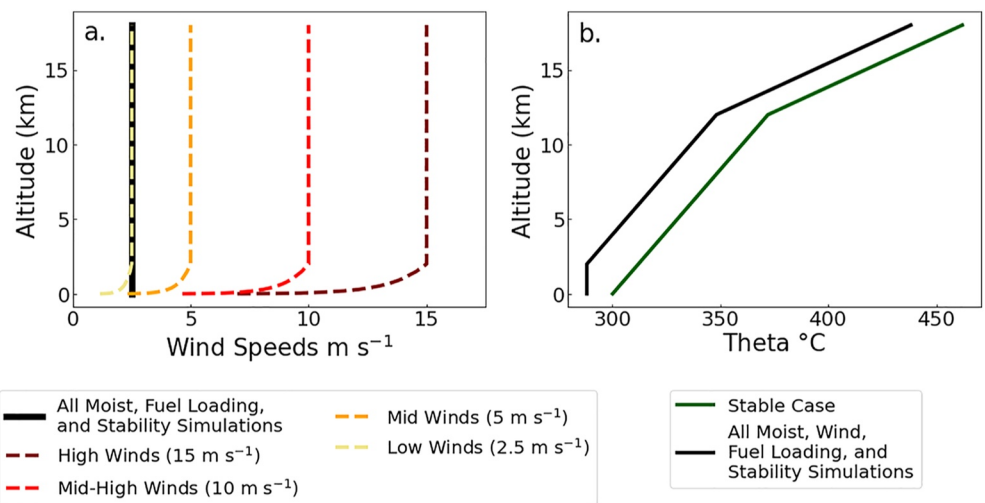


Figure 2. Input geostrophic wind (a) and potential temperature (b) profiles.

Soundings for the four moist profiles, of which only MR75 develops any convective available potential energy (CAPE) after spinup, are presented in Figure 3. CAPE is a measurement of a parcel's potential energy for rise after it reaches the free troposphere, and it is generally used as a metric for the development of deep convection (Fritsch & Chappell, 1980; Moncrieff & Miller, 1976). Before ignition, MR75 has a small average CAPE value in the background atmosphere of $41.26 J kg^{-1}$; the rest of the simulations have a CAPE value of 0. Upon ignition, a small amount of fuel moisture (defined as 8% of the fuel content) is released into the atmosphere in all cases (dry and moist), and CAPE then develops (or develops further) specifically in the convection column above every fire. Of note is that the boundary layer height slightly decreases (by around 100 m) for MR75 after spinup, as the simulation begins to develop stratification around an altitude of 1.9 km. The other three simulations see an increase in boundary layer height of around 200 m each.

Following spinup, either a 2-km radius or 4-km radius fire is defined in the center of the nest, and the entire area is lit (the fire spreads outward from the center point throughout each specified ignition area within seconds, mimicking an areal ignition). For all cases, the fire burns for the same amount of time—1.5 hr. In the high-wind

Table 2
Simulation Overviews

Simulation	Label	Wind speed	ABL stability	Moisture	Radiation	ABL shear	Relative humidity
Low winds	LoWi	2.5 $m s^{-1}$	Neutral	Dry	No	Yes	0%
Mid winds	MedWi	5 $m s^{-1}$	Neutral	Dry	No	Yes	0%
Mid-high winds	MiHiWi	10 $m s^{-1}$	Neutral	Dry	No	Yes	0%
High winds	HiWi	15 $m s^{-1}$	Neutral	Dry	No	Yes	0%
Base	Base	2.5 $m s^{-1}$	Neutral	Dry	No	No	0%
50% RH	M50	2.5 $m s^{-1}$	Neutral	Moist	No	No	50%
25% RH + radiation	MR25	2.5 $m s^{-1}$	Neutral	Moist	Yes	No	25%
50% RH + Radiation	MR50	2.5 $m s^{-1}$	Neutral	Moist	Yes	No	50%
75% RH + Radiation	MR75	2.5 $m s^{-1}$	Neutral	Moist	Yes	No	75%
Stable	Stable	2.5 $m s^{-1}$	Stable	Dry	No	No	0%

Note. Each column lays out the input parameters for the simulations. When referenced elsewhere, each label is followed by an underscore and the fire radius. For example, the base case for the 2-km radius fire will be referred to as Base_2. "Moist," as used in describing the simulations, refers specifically to the addition of background atmospheric humidity (as opposed to a simulation initialized in a completely dry state). Once the fire is lit, all simulations see some release of moisture from the fuel source

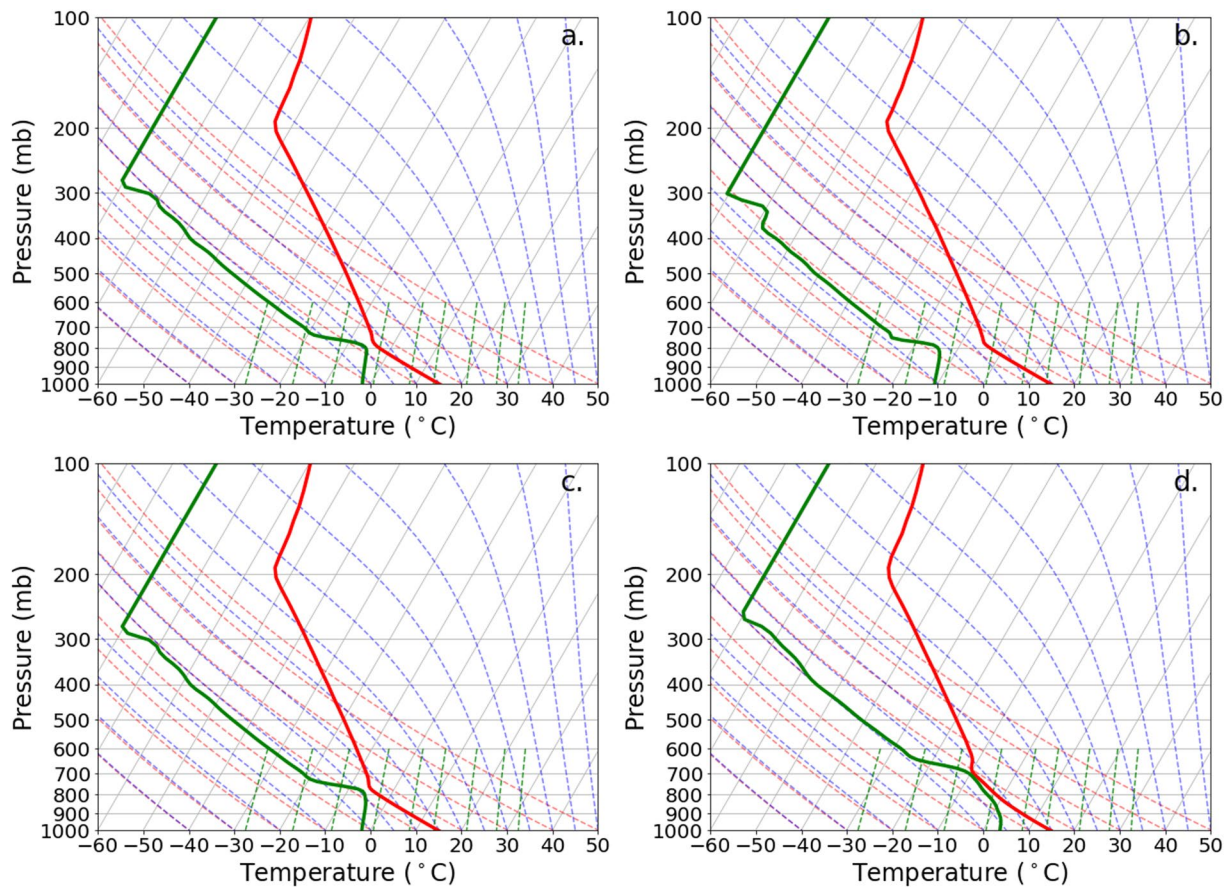


Figure 3. Post-spinup soundings for the four moist cases: M50 (a), MR25 (b), MR50 (c), and MR75 (d). Green indicates the dew point temperature profiles, while red indicates the environmental temperature profiles.

case (HiWi), the fire reaches the domain edge at this point, so the other cases are terminated at the same time to facilitate comparison.

2.3. Fuel Source

A nuclear weapons strike would cause an areal ignition of the strike area. Key military bases, population-dense cities, or other strategic and anthropogenically-developed locations—all having dense fuel loads—would be likely targets. Observations from World War II, during which over 60 fires were started by incendiary bombing, suggest that firestorms, which generate strong enough convection to loft a great amount of smoke into the upper troposphere, can develop when the fuel loading exceeds 4 g cm^{-2} (Glasstone & Dolan, 1977). Another study simulating the Hamburg firestorm of WWII used a fuel loading of about 2.6 g cm^{-2} (Penner et al., 1986)—about two times as large as ours. For our simulations, we use heavy logging slash as the fuel bed, which has a smaller loading of 1.3 g cm^{-2} . Because WRF-Fire has been developed as a wildland fire parameterization, its fuel sources are taken from the Anderson 13 Standard fuel categories (Anderson, 1982), and heavy logging slash is the densest option available. By the aforementioned standards, therefore, firestorm development is not possible. However, WRF-Fire is still able to model pyroconvection, which can transport aerosols into the UTLS, as this can occur in situations with wildland fuel loading (Fromm et al., 2010; Luderer et al., 2006; Peterson, Hyer, et al., 2016; Trentmann et al., 2006). And, our fuel bed is denser than the 0.91 g cm^{-2} (Robock, Toon, Bardeen, et al., 2019) that was used in Reisner et al. (2018).

WRF-Fire considers the fuel source to be 100% combustible, with 2% of it forming PM_{2.5} smoke, which then is transported through the domain as a passive tracer. To calculate the smoke profile, all smoke that has exited the domain must be accounted for. An estimate of total smoke (in and out of the domain) at each height can be

calculated by assuming that all smoke at the edges of the domain will exit by the next output write time. This time interval has been selected independently for each simulation to minimize error between the smoke generated (an aggregate model variable that updates each time step) and the estimated smoke presence. For the final smoke profile, the smoke is assumed to remain fixed in the vertical after it exits the domain. To calculate the error at each vertical level, the percentage difference between the total smoke generated and the total calculated smoke in (and exited from) the domain is multiplied through the values at each height. This difference is less than 5% for all cases.

2.4. Model Uncertainty

WRF-Fire is under ongoing development; therefore, it has some limitations that could lead to either underestimation or overestimation of smoke profile concentrations. As the smoke is a passive tracer, it does not seed cloud development, nor is smoke scavenged out of the atmosphere via rainfall (both factors leading to overestimation of smoke). Oxygen starvation, which would limit fuel burned or prolong the period of burning, is not considered but is discussed in Section 3.1 (overestimation). Lightning, which could spark new ignitions, is not simulated (leading to an underestimation of burn area and, therefore, smoke). The wildland fuel density used here is lower than that of urban fuels (underestimation), but the fuel bed is being modeled as continuous, without breaks in the source (overestimation). The fuel burns quicker than urban fuels, leading to an initial burst of heat release and initial lofting, followed by a tapering once the ignition area has burned out, which does not mirror what has been modeled in past studies focused on nuclear winter (underestimation). The fire parameterization has been developed for perimeter and point fires, not areal ignitions as is prescribed in this study (unsure of the consequences). Long-range fire spotting, otherwise known as branding and a method of fire propagation (Koo et al., 2010; Tarifa et al., 1965), is not currently supported by the model (underestimation). Finally, smoke does not interact with radiation to enable self-lofting behavior (underestimation of lofting and residence time) (Mills et al., 2014, 2008; Robock, Oman, Stenchikov, et al., 2007; Yu et al., 2019). All of these elements of uncertainty must be taken into consideration when examining the results of these simulations.

3. Results

The amount of smoke injected into the UTLS determines the amount of smoke that may ultimately rise above the tropopause, given enough time and radiative heating. Although not considered here, this process can be simulated in climate models, as shown in Toon et al. (2019), where smoke injected between 3.5 and 7 km below the tropopause ultimately ascended into the stratosphere. To assess the impacts of local meteorological conditions on smoke transport into the UTLS, we quantify the vertical smoke profile (integrated over the x-y plane to yield Mg km^{-1} of altitude). First, however, we present an analysis of potential oxygen starvation in the model. Following that is analysis of the smoke profile, and finally we address metrics—vertical velocity, CAPE, and horizontal wind speeds—that may be used at the time of combustion to ascertain how high the plume could rise.

3.1. Oxygen Starvation in the Model

One point of concern in modeling large fires is the potential for oxygen starvation. For combustion to occur, a fuel source, a heat source, and oxygen must all be present. Once the amount of oxygen in air drops below 16%, however, fires can no longer be sustained. Models that do not incorporate chemistry interactions, including WRF-Fire, typically do not consider the potential for oxygen depletion. Therefore, particularly intense simulated fires may not be physically viable. The initial amount of oxygen in a grid cell with an active fire, combined with the convergence of surrounding air into the fire center, must be large enough to support the heat release and burn rate being simulated.

To check for oxygen starvation, the mass of oxygen initially present in the lowest two grid cells (ground to 200m) is first calculated according to Equation 1, with an assumed simplified air composition of 79% nitrogen (F_{N_2}) and 21% oxygen (F_{O_2}) by volume. The molar mass of O_2 is 32 g mol^{-1} (M_{O_2}) and the molar mass of N_2 is 28 g mol^{-1} (M_{N_2}). Air pressure (P) is given in units of Pa. Each element of the equation is given at the grid cell on the fire mesh with the location (i, j) at time t .

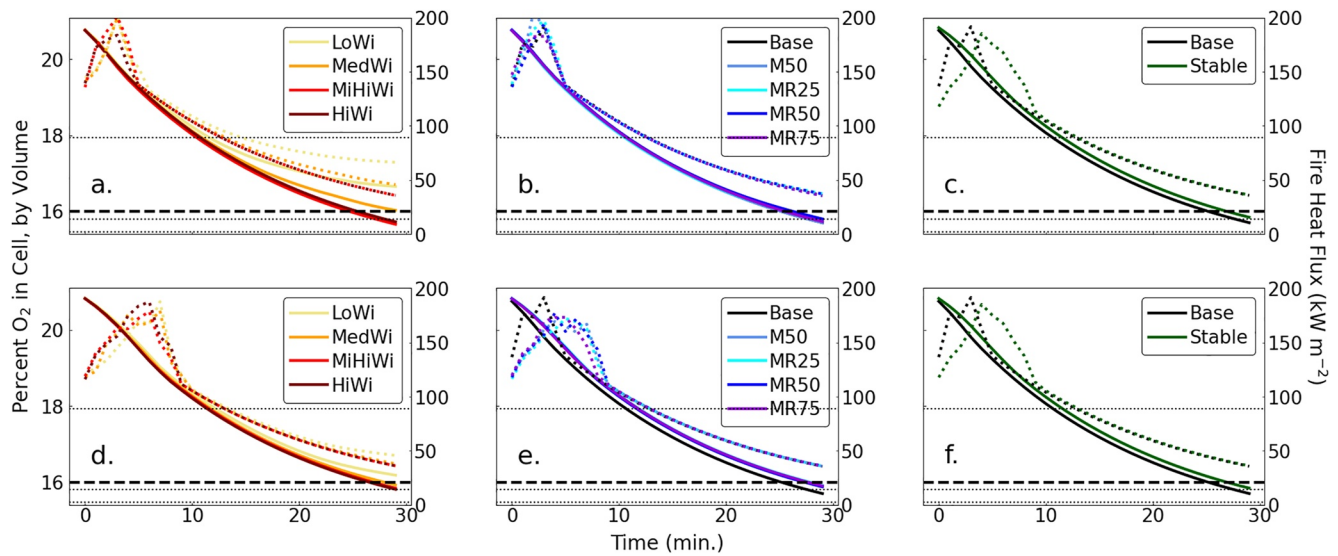


Figure 4. Top: Average oxygen depletion in the lowest 200 m of the model across burned area, assuming no air replenishment (left axis, solid), and heat release rate (kW m^{-2}), right axis, dotted) for the 2-km ignition radius fires, grouped by simulation subset (a) Winds, (b) Moisture, and (c) ABL Stability. Bottom: Average oxygen depletion in the lowest 200 m of the model across burned area, assuming no air replenishment (left axis, solid), and heat release rate (kW m^{-2}), right axis, dotted) for the 4-km ignition radius fires, grouped by simulation subset (d) Winds, (e) Moisture, and (f) ABL Stability. The heat release rates for each of Penner et al. (1986)'s three fire simulations are marked in each plot by horizontal dotted lines ($\text{HRR} = 2.2, 14, \text{ and } 89 \text{ kW m}^{-2}$). The 16% depletion threshold is depicted via a thick, horizontal, dashed line on each plot.

$$O_{2,\text{present},ijt} = \left(\frac{dP_{ijt}}{g} \right) (dx_{ij})(dy_{ij}) \frac{1}{(M_{O_2})(F_{O_2}) + (M_{N_2})(F_{N_2})} M_{O_2} F_{O_2}. \quad (1)$$

The combustion of oxygen is a function of heat release rate. Both Huggett (1980) and Thornton (1917) found an average heat release rate (HRR_{avg}) of $13.1 \text{ MJ kgO}_2^{-1}$ for the burning of organic solids. This constant is used to determine the amount of oxygen consumed in accordance with the fire's heat release rate. The oxygen depletion over time is calculated using linear interpolation between heat release rates on 1-min outputs, with a model time step (Δt) of 0.1 s. The consumption of oxygen per time step is calculated in Equation 2. HRR_{ij} , the heat release rate in each ignited grid cell, is given in W m^{-2} . The variables dx_{ij} and dy_{ij} refer to each cell's extent in the x and y directions.

$$O_{2,\text{cons},ijt} = \sum_{n=0}^{(\Delta t * 600s) - 1} \frac{1}{\text{HRR}_{\text{avg}}} (dx_{ij})(dy_{ij})(\Delta t) \left((\text{HRR}_{ij,t+1} - \text{HRR}_{ij,t}) \left(\frac{n}{\Delta t * 600s} \right) + \text{HRR}_{ij,t} \right). \quad (2)$$

The oxygen consumed by combustion is subtracted from the oxygen originally present in the cell each time step, resulting in a cumulative depletion of oxygen. Replenishment of air via inflow to the area is not considered in Equation 2; however, oxygen is assumed to be consumed during this time within a 200-m deep layer.

The most intense heat release occurs during the initial areal ignition of the fires. When lit, the fire rapidly consumes all of the fuel in the specified ignition area, and what remains following this fuel burnout is a perimeter fire with a much lower HRR. This process of bulk, rapid fuel consumption takes about four minutes for the 2-km radius fires, and about 7 min for the 4-km radius fires (Figure 4). The greatest oxygen consumption occurs during this time.

Assuming a well-mixed boundary layer during and following ignition, we can infer a 30-min turnover time in the vertical for the lowest 2 km of the model. Therefore, we have only plotted oxygen depletion for this time period in Figure 4 and assume that turnover following the initial ignition will suffice to maintain burning in what eventually becomes, for all cases, a perimeter fire. O_2 levels drop to just below 16%, the amount necessary for sustained burning, by minute 30. However, by looking at a cross-sectional plot of winds during this time (Figure 5), we see that O_2 is in fact replenished by horizontal flow into the burn area, at velocities of up to 15 m s^{-1} . With this

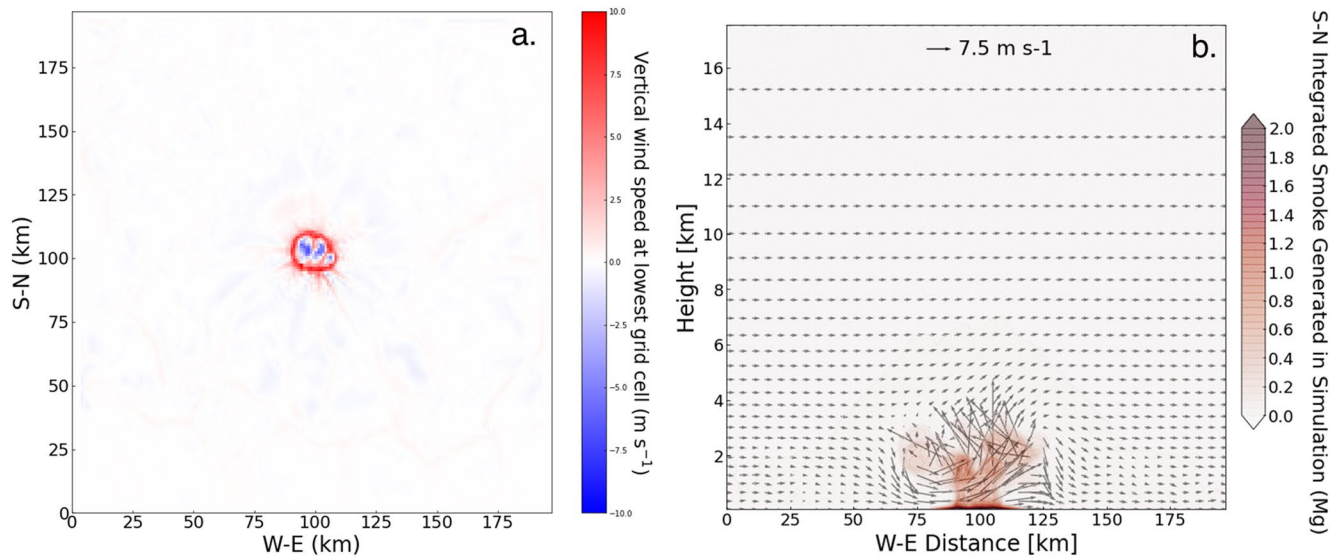


Figure 5. Left: Planar view of vertical velocities for Base_2 shortly after ignition. Right: Vertical cross-section of the nest for Base_2 shortly after ignition, with contours indicating smoke content and arrows indicating winds.

inflow and considering a full vertical turnover of air in the boundary layer after 30 min, oxygen starvation will not be a factor limiting fuel burn.

3.2. Smoke Lofting

Quantification of how meteorology affects the altitude of smoke lofting can help better inform assessments of pyrocumulus risk in fire forecasting models and the radiative impacts of large fires in climate models. Therefore, the primary interest of this study is evaluating the sensitivity of smoke lofting to local weather conditions. Here, we examine how varying wind speeds, boundary-layer stability, and moisture affect the immediate rise, or injection height, of smoke. In general, higher wind speeds dampen lofting by dispersing smoke horizontally,

moisture enhances plume rise due to latent heat release, and a thermally neutral, dry boundary layer provides better conditions for deeper ascension than a thermally stable, dry boundary layer. In particular, the presence of moisture has the greatest impact on smoke lofting (by enhancing it) as compared with the other two atmospheric parameters. Excluding it from applied fire simulations, as in Reisner et al. (2018), therefore, runs the risk of generating erroneous conclusions.

The amount of smoke that reaches the UTLS in each simulation in this study is presented in Table 3 for the 2-km radius fires and Table 4 for the 4-km radius fires.

3.2.1. Wind Speeds

Previous studies suggest that background wind speeds will affect whether a mass fire develops as a conflagration or as a firestorm—the latter of which can generate strong enough convection to inject smoke into the UTLS. One observational study from WWII suggests that an ambient wind speed of 8 mph, or roughly 3.6 m s⁻¹, is the tipping point between conflagration and firestorm development (Rodden et al., 1965). Slower winds favor the firestorm, while faster speeds favor a conflagration. Due to our lower fuel loading, we do not see development of a firestorm in our LoWi cases. That is, we do not see winds flowing into the fires center from all radial directions, even during ignition.

Table 3
Smoke Generation, Upper Troposphere and Stratospheric Smoke Lofting, With the 2-km Radius Ignition Area

Simulation	Total smoke (Mg)	Smoke above 9 km (Mg)	Smoke above 9 km (%)	Smoke above 12 km (Mg)	Smoke above 12 km (%)
LoWi_2	5.1E3	597.1	11.65	77.4	1.51
MedWi_2	6.1E3	40.9	0.67	0.12	0.00
MiHiWi_2	1.0E4	2.2	0.02	0.00	0.00
HiWi_2	9.0E3	3.9	0.04	0.00	0.00
Base_2	4.9E3	719.8	14.53	22.8	0.46
M50_2	5.7E3	1.79E3	31.25	144.7	2.53
MR25_2	5.9E3	688.7	11.6	15.5	0.26
MR50_2	5.8E3	1.33E3	22.94	126.5	2.19
MR75_2	6.2E3	2.8E3	44.92	846.6	13.6
Stable_2	4.6E3	255.01	5.53	13.1	0.28

Note. Negative error values indicate an overestimation of total smoke in the atmosphere, compared with actual smoke generation at the surface, while positive values indicate an underestimation

Table 4
Smoke Generation, Upper Troposphere and Stratospheric Smoke Lofting, With the 4-Km Radius Ignition Area

Simulation	Total Smoke (kg)	Smoke above 9 km (kg)	Smoke above 9 km (%)	Smoke above 12 km (kg)	Smoke above 12 km (%)
LoWi_4	2.1E4	732.9	3.54	71.0	0.02
MedWi_4	2.4E4	751.2	3.09	16.9	0.01
MiHiWi_4	3.3E4	232.5	0.70	3.0	0.07
HiWi_4	3.3E4	252.4	0.76	6.0	0.34
Base_4	1.9E4	1.13E3	5.94	389.3	2.05
M50_4	2.3E4	4.95E3	21.9	528.5	2.34
MR25_4	2.0E4	2.02E3	10.15	287.3	1.44
MR50_4	2.2E4	5.22E3	23.4	920.8	4.13
MR75_4	2.4E4	7.02E3	28.88	1.35E3	5.57
Stable_4	1.8E4	739.9	4.0	351.4	1.9

Note. Negative error values indicate an overestimation of total smoke in the atmosphere, compared with actual smoke generation at the surface, while positive values indicate an underestimation

In four simulations for each ignition radius, we vary the geostrophic wind speed between 2.5 and 15 m s⁻¹. These simulations are initialized with wind speeds increasing through the ABL, which are then held constant above the top of the boundary layer. The forcing wind speed profiles are shown in Figure 2. In all cases, there is no specified wind directional shear, except for that which arises due to the Coriolis force (with a Coriolis parameter assumed to be 10⁻⁴ s⁻¹ for a mid-latitude location) and frictional forces.

3.2.1.1. 2-km Radius Fire

In this set of simulations, the vertical smoke profiles in the 2-km radius fire 1.5 hr (50 min in the case of HiWi_2) after fire initiation demonstrate the impact wind speeds have on lofting (Figures 6a and 6b). The largest amount of smoke generation occurs in MiHiWi_2, as the faster winds cause the fire to spread more rapidly over the course of the simulation, therefore, burning a larger swath of land. Despite the even higher wind speeds of HiWi_2, its burn area is not the largest because the simulation terminates in about half the time of the other three cases. In spite of their relatively greater amounts of smoke generation in these two cases, they both return a negligible amount of smoke above the tropopause, as their strong horizontal winds prevent deep vertical motion (Figure 7b). MiWi_2 shows similarly insignificant results. Conversely, LoWi_2 results in a much greater amount of upper tropospheric smoke presence (Figures 6a and 6b), with a total of 11.65% penetrating the tropopause (Table 3 and Figure 7a).

These results concur with previous studies, using coarser simulations, evaluating the impact of horizontal wind speeds on plume rise. Graf et al. (1999) and Freitas et al. (2010) both found that strong winds inhibit plume rise. Freitas et al. (2010) attributed this dampening to drag and increased entrainment of cooler air into the plume area. The entrainment of cooler air into the convection column at higher altitudes, five minutes after ignition in HiWi_2 versus LoWi_2, is shown in Figure 8. There is strong entrainment into the convection column up to 4 km for HiWi_2 (Figure 8a), in particular on the upwind side of the fire, while at the same altitude, LoWi_2 displays outflow (Figure 8b). The air directly above HiWi_2 is much cooler than that of LoWi_2, while the temperature upwind is higher in HiWi_2 (Figure 8d), indicating entrainment from that side of the fire into the plume. Smoke differences above the fires five minutes after ignition (Figure 8c) already suggest what will ultimately amount to LoWi_2 injecting a larger smoke mass into the UTLS.

3.2.1.2. 4-km Radius Fire

All cases in the 4-km wind variability simulations result in a greater amount of smoke reaching the UTLS than in the 2-km radius fire, as the increased surface heat flux from the larger ignition area results in stronger convection. As with the 2-km radius fire, the smallest amount of smoke generation and the largest percentage of UTLS smoke injection for this subset occurs in the lower wind speed case (LoWi_4). However, compared with the 2-km radius fire, a smaller percentage of total smoke production reaches the upper troposphere—3.54%, as compared with 11.65% (Figures 6b and 6c). Despite a 400% increase in the ignition area of the larger fire, the total amount of smoke reaching the upper troposphere and stratosphere increases by 135.8 kg or only 123%. Additionally, the percent smoke reaching the stratosphere decreases to nearly 0%, despite this overall increase in total smoke above the tropopause (Table 4).

The three other wind speed cases—MedWi_4, MiHiWi_4, and HiWi_4—also see an increase in percent smoke rise into the upper troposphere and stratosphere with the larger ignition area. MedWi_4 in particular returns in a greater amount of upper troposphere plume presence when compared with the 2-km radius simulation, with an over 450% boost. Presumably the stronger convection resulting from the larger ignition area—amounting to an increase of 47 GW, or around double the power output of the 2-km radius fires—provides enough energy for these fires to overcome the dampening effect of the stronger horizontal winds and inject more smoke above the inversion at the tropopause.

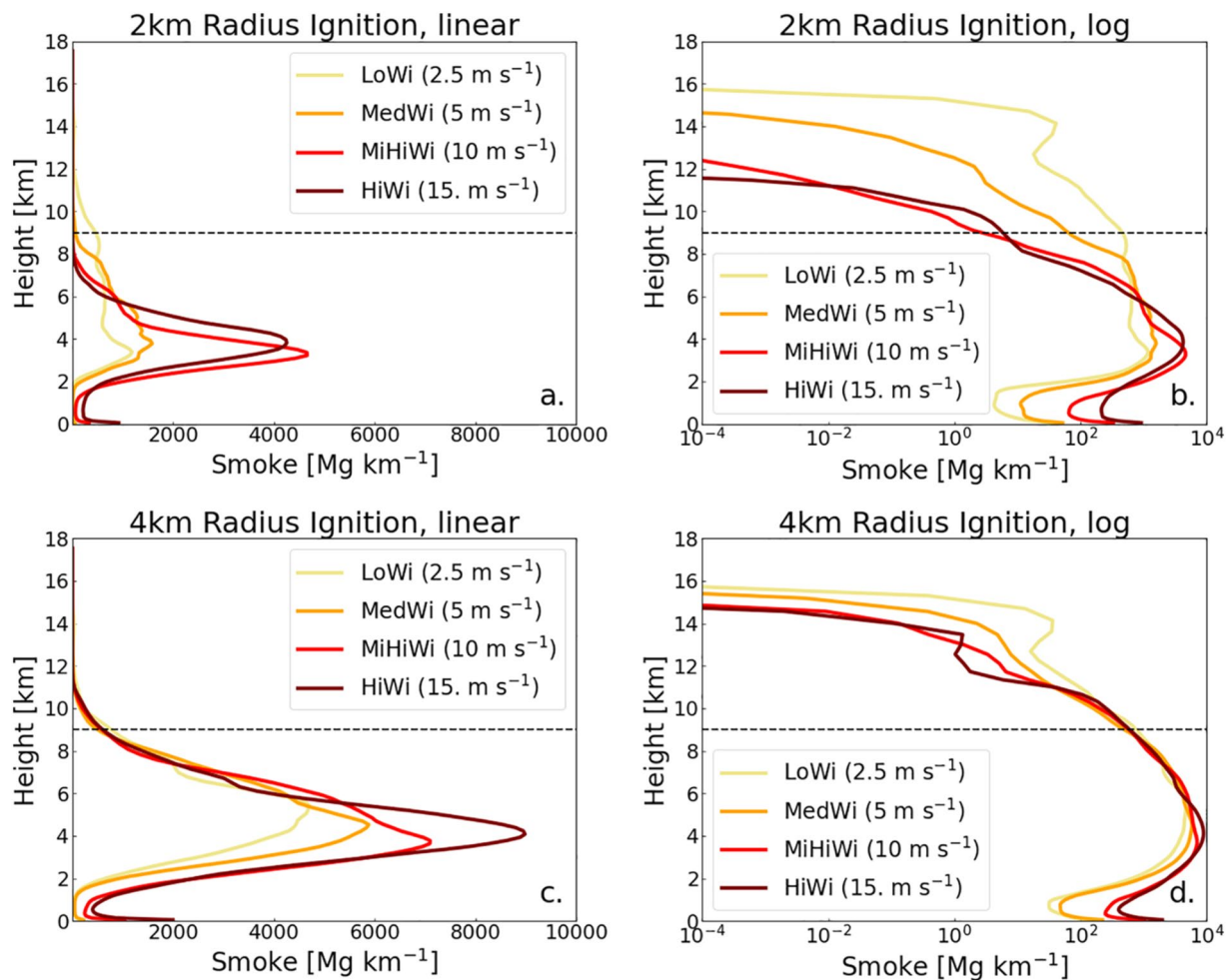


Figure 6. Final profiles of vertical smoke distribution (in Mg km^{-1}) for the wind simulations after 1.5 hr of burning. Linear plots (a) and (c) and logarithmic plots (b) and (d), for the 2 km radius (a) and (b) and 4 km radius (c) and (d) ignitions are shown.

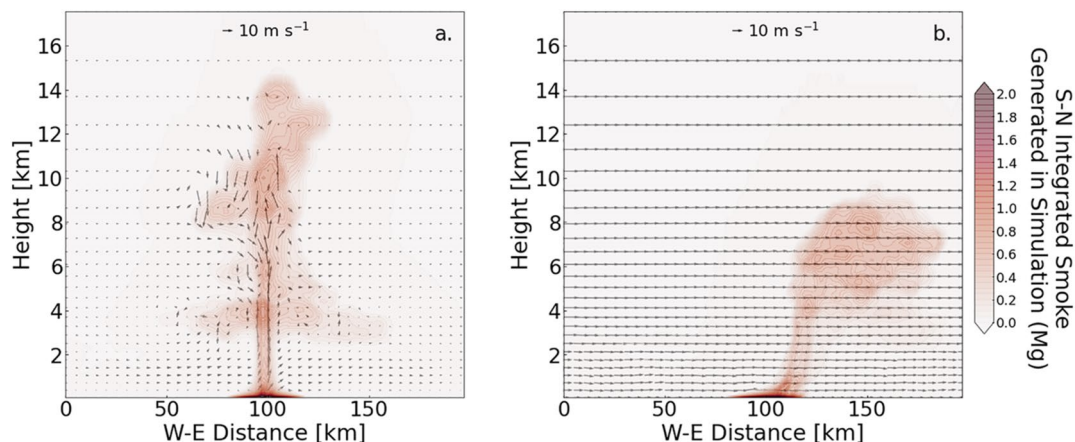


Figure 7. Cross-sectional winds taken from a W-E transect through the domain center, with integrated smoke (colored contours), for LoWi_2 (a) and HiWi_2 (b). Stronger horizontal winds in HiWi_2 dampen the convective lofting of smoke.

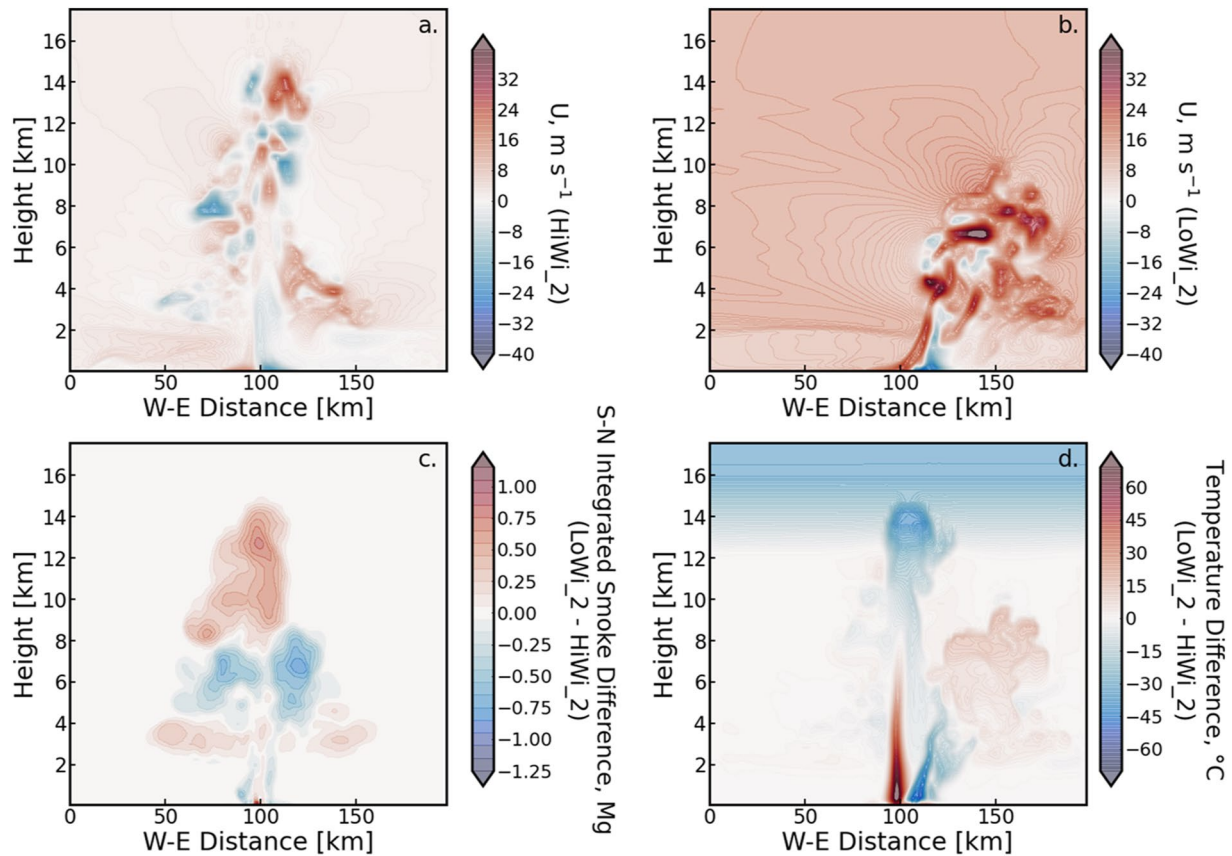


Figure 8. Vertical cross-sectional profiles of U for (a) LoWi_2 and (b) HiWi_2, (c) smoke differences (LoWi_2 - HiWi_2), and (d) temperature differences (LoWi_2 - HiWi_2) 10 min after ignition.

3.2.2. Moisture and Radiation

The inclusion of moisture and a radiation scheme in the model is important for a realistic simulation. Evaluating the impact of water vapor can provide an insight into how significant a role it plays in smoke lofting. The ignition of vegetation releases moisture that can contribute to cloud formation, but the addition of water vapor introduces the potential for pyrocumulonimbus formation, which has been shown to inject smoke into the stratosphere (Fromm et al., 2010).

In each of the three simulations for each ignition radius, background moisture is uniformly set at a constant 25%, 50%, or 75% relative humidity throughout the entire 3D domain, with the RRTMK radiation parameterization enabled. Of note is that the global average humidity in the boundary layer is around 75%. In addition to these simulations, another case with 50% relative humidity is run without any radiation considered. These simulations are compared alongside the base case, which is dry and does not include radiative effects (Figure 9). All simulations have constant 2.5 m s⁻¹ winds throughout the domain and a thermal profile mirroring that of the base scenario.

3.2.2.1. 2-km Radius Fire

In general, adding moisture into the atmosphere enhances air parcel ascent, as that moisture releases latent heat when it rises and condenses. If cloud droplets rise high enough, they freeze into ice—a process that also releases heat. When radiation is considered, a slightly cooler troposphere, as compared with the M50 cases, develops during spinup. Because of this, we see deeper convection for MR50_2 once the fire is lit, leading to a greater amount of precipitation (here, precipitation is the combination of rain and graupel). Since our passive smoke tracer follows the dynamics of the atmosphere, smoke follows the precipitation out of the upper troposphere, leading to a reduced amount of smoke above 9 km and above 12 km by the simulations' end (Figure 10a). Similarly, we see a smaller smoke injection above 9 and 12 km for MR25_2 compared with Base_2. This occurs, again, due to the effects on smoke by precipitation. Base_2 sees no precipitation development, whereas MR25_2 does, and as

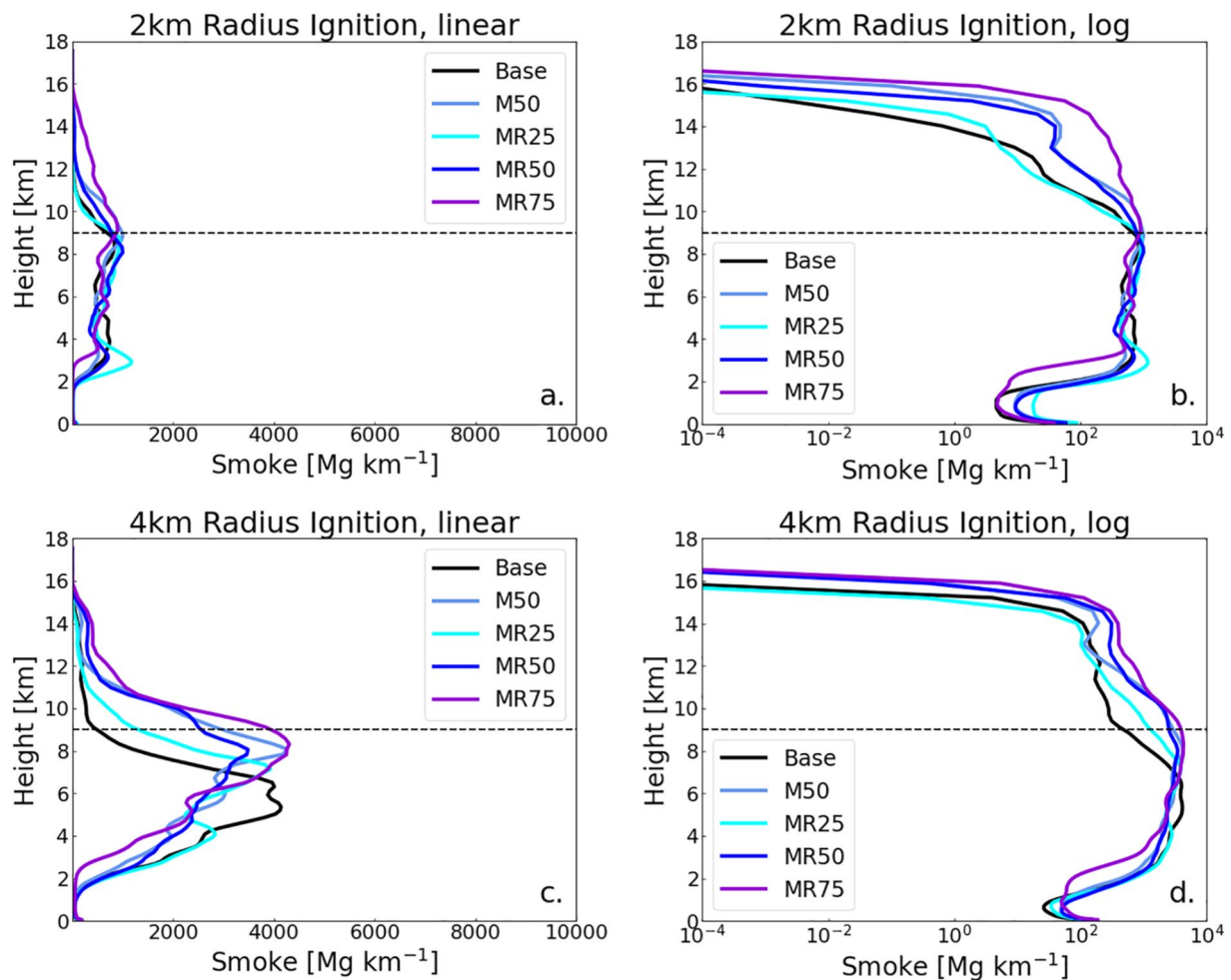


Figure 9. Final profiles of vertical smoke distribution (in Mg km^{-1}) for the moist simulations after 1.5 hr of burning. Linear plots (a) and (c) and logarithmic plots (b) and (d), for the 2 km radius (a) and (b) and 4 km radius (c) and (d) ignitions are shown.

a result a greater amount of smoke exits the upper troposphere and stratosphere in MR25_2, as compared with Base_2 (Figure 10b).

M50_2 lofts over 31% of its smoke production into the upper troposphere, while MR50_2 injects only 23% that high. Similarly, Base_2 results in a 14.5% plume rise above 9 km, while MR25_2 only convects 11.6% to that level. Still, when comparing all the cases using a radiation scheme, an increase in environmental humidity results in an increase in the amount of smoke reaching the upper troposphere. MR75_2 sees the greatest amount of smoke lofting of all the 2-km radius ignition simulations, with nearly 45% extending above 9 km and 13.6% rising into the stratosphere (Table 3, Figures 9a and 9b).

3.2.2.2. 4-km Radius Fire

When the fire radius is increased to 4 km, the precipitation difference between MR50_4 and M50_4 is smaller than that between MR50_2 and M50_2 (Figure 10). Therefore, the amount of smoke that is removed from the upper troposphere via downdrafts becomes comparable. Additionally, with radiation enabled in MR_50, deeper convection occurs. As a result, MR50_4 injects a greater amount of smoke above 9 km than M50_4 (23.4%, compared with 10.2%). Likewise, even though Base_4 does not develop precipitation while MR25_4 does, the stronger convection with the larger fire size, deepened by the increased latent heat release in MR25_4, lofts enough smoke above 9 km that even with rainout more smoke still remains in the upper troposphere in MR25_4 (10.5%) than in Base_4 (5.94%).

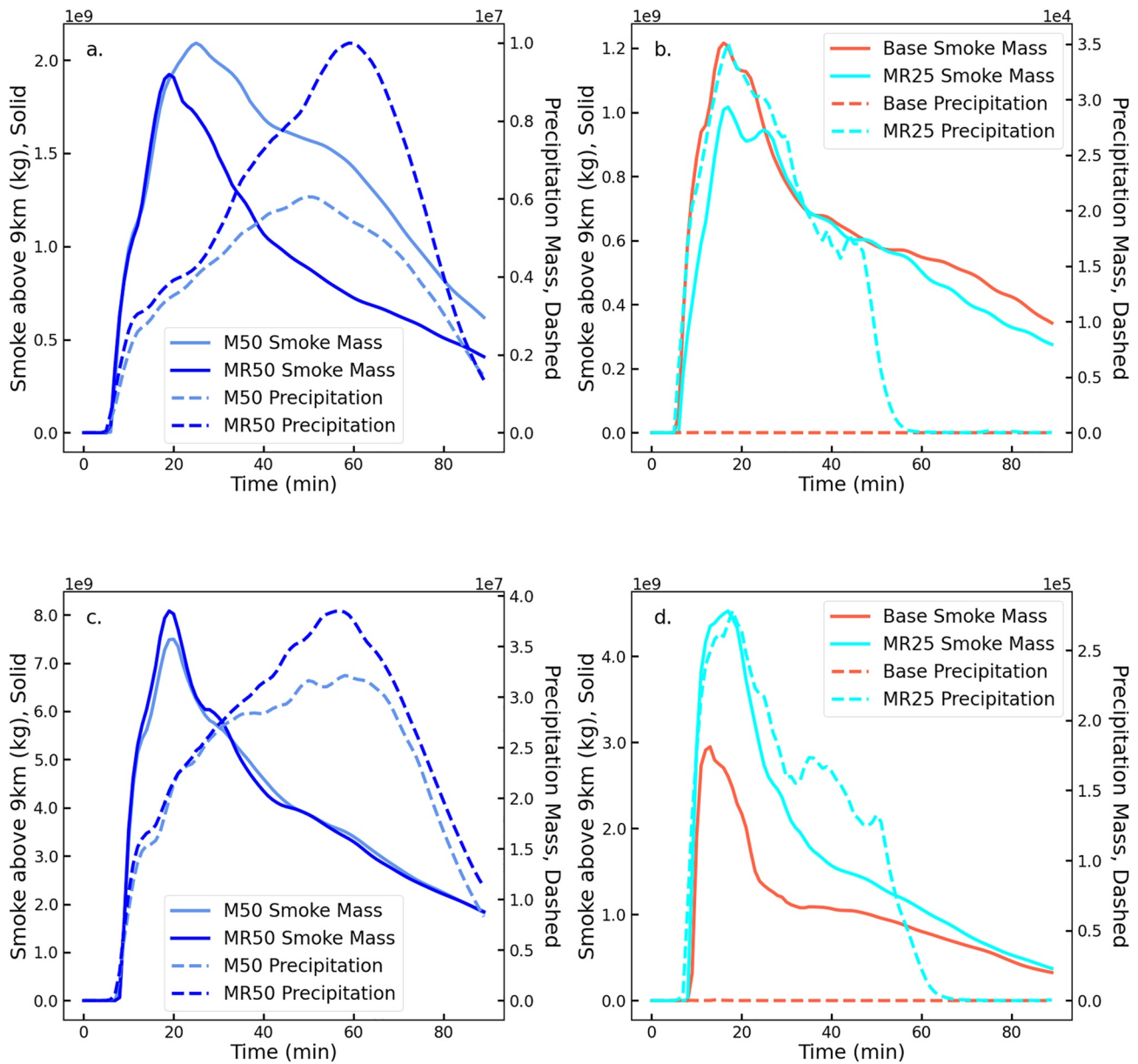


Figure 10. Time series of total smoke above 9 km (solid) and precipitation in the domain (dashed) for (a) M50_2 and MR50_2, (b) Base_2 and MR25_2, (c) M50_4 and MR50_4, and (d) Base_4 and MR25_4.

MR75 lofts the most smoke of all the simulations, at almost 29% above 9 km and 5.6% above 12 km for MR75_4, followed by the less humid cases (MR25, MR50, and M50) in accordance with their water vapor content (Table 4). Despite significant increases in the total smoke rise, the overall percent plume rise above 9 and 12 km for all the moisture cases is lower for the 4-km radius fire than for their counterparts with the 2-km radius fires (Tables 3 and 4).

Following these findings, we may also conclude that even though aerosol scavenging effects (i.e., cloud seeding by combustion byproducts) are not explicitly modeled by WRF, the effect of scavenging is still somewhat represented due to the parcel-following behavior of the passive smoke tracer. As downdrafts fall, for example, smoke falls with it.

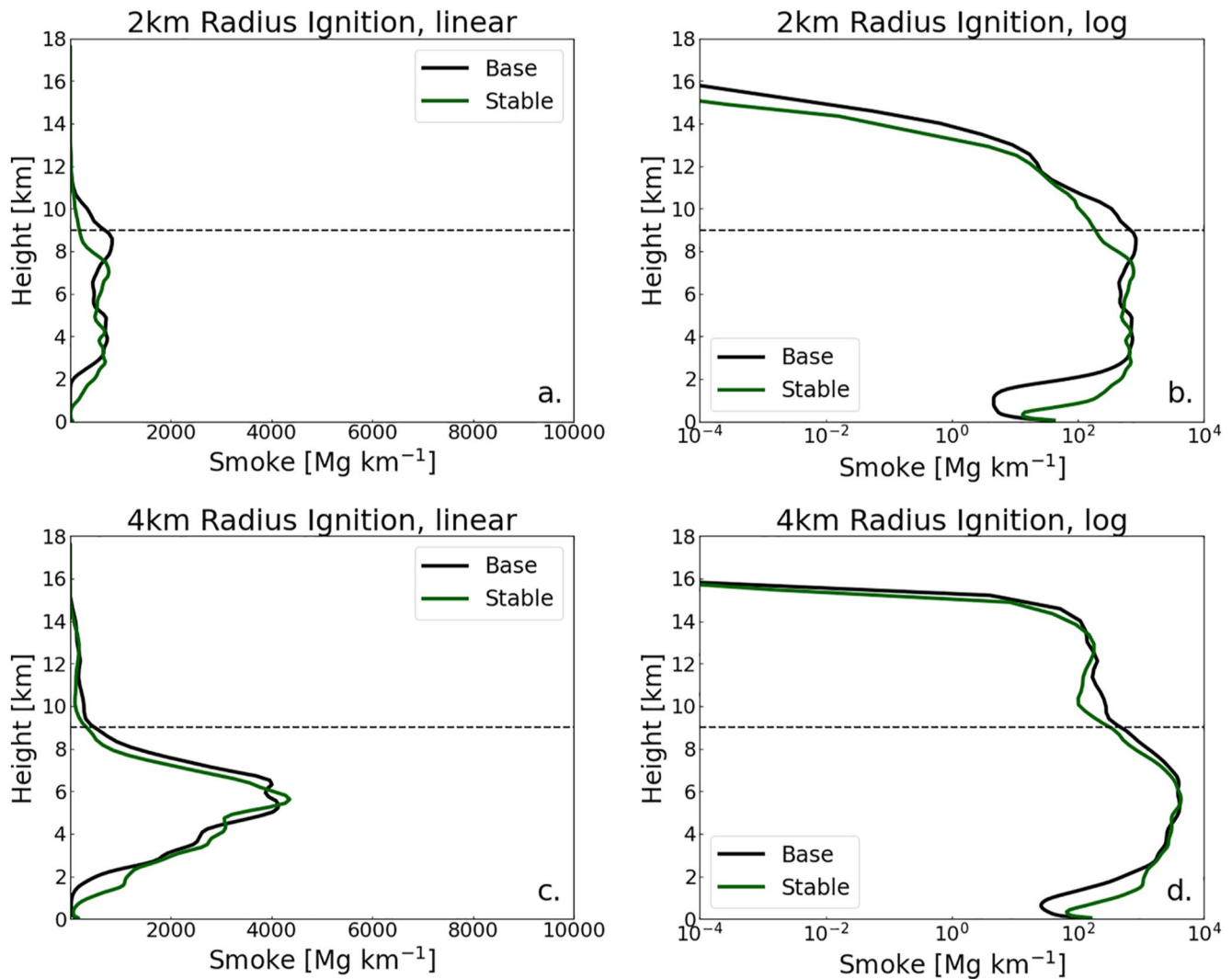


Figure 11. Final profiles of vertical smoke distribution (in Mg km^{-1}) for the stability simulations after 1.5 hr of burning. Linear plots (a) and (c) and logarithmic plots (b) and (d), for the 2 km radius (a) and (b) and 4 km radius (c) and (d) ignitions are shown.

3.2.3. Atmospheric Boundary Layer Stability

ABL stability, hereafter also referred to as atmospheric stability, may enhance or reduce a large fire's intensity, which in turn affects the probability it will mature into a firestorm (Cotton, 1985; Penner et al., 1986). A stable atmosphere dampens plume rise, while a more convective atmosphere can enhance lofting potential. Two cases—neutral (the base case) and stable—have been selected to evaluate this theory. Both have a stable free troposphere, with varying stability in the 2-km deep boundary layer. In the case of both fire sizes, we find that boundary-layer stability exerts a modest influence on the smoke distribution.

With the smaller ignition radius and, therefore, the lower heat release, the stable boundary layer dampens plume rise. Compared with Base₂, which lofts over 14% of the smoke generated into the upper troposphere and stratosphere, Stable₂ is only able to inject 5.53% that high (Table 3, Figures 11a and 11b). However, when the fire radius is increased to 4 km, the difference between the two cases' lofting capabilities shrinks and Base₄ lofts only 1.9% more smoke above 9 km than Stable₄ (Table 4, Figures 11c and 11d). We conclude that, as with the moisture variability, the heat release associated with the larger fire size can overwhelm the influence of atmospheric stability.

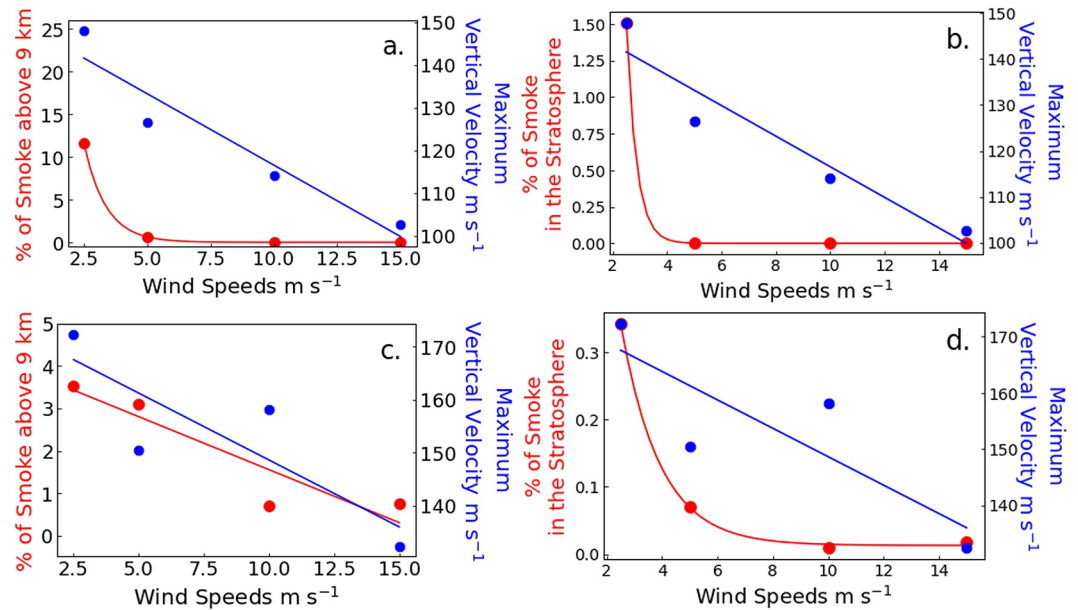


Figure 12. Percent of smoke reaching the upper troposphere (a) and (c) and stratosphere (b) and (d) compared with wind speeds (red) and maximum vertical velocity in the domain compared with wind speeds (blue), for the 2-km radius ignition (a) and (b) and the 4-km radius ignition (c) and (d).

3.3. Relative Importance of Moisture and Winds

Certain metrics can give us an insight into which atmospheric factors more strongly affect the depth of smoke lofting from a fire. Horizontal wind speeds, vertical velocity, and CAPE facilitate comparative analysis among fires in varying atmospheric conditions to evaluate in which scenarios more smoke may rise high in the atmosphere.

3.3.1. Horizontal Wind Speeds and Vertical Velocity

The simulations for both the 2-km radius and 4-km radius fires have shown that, with both fire sizes, the horizontal wind speeds will influence vertical velocity and, therefore, the total amount of smoke reaching the upper troposphere and stratosphere. With the smaller fire, which has a weaker heat flux and slower vertical velocities (w), horizontal winds can more easily mix the plume out lower in the atmosphere (Figure 7). Therefore, the stronger the horizontal winds, the less smoke will be lofted. A trend emerges between vertical velocity and horizontal wind speeds (Figure 12) as they are negatively correlated. This relationship is stronger for the smaller fire; as previously discussed, with enough power (as with the 4-km radius fire), the generated convection will begin to overcome the impact of these horizontal winds. And, similarly, vertical velocity and smoke above 9 km also have a negative correlation (Figure 12a).

Rodden et al. (1965) posed a threshold wind for firestorm development, at 8 mph or 3.58 m s⁻¹. Interestingly, this value appears to be relevant in our simulations, as it falls in the middle of the wind speeds for LoWi and MedWi, between which there is a sharp drop in smoke lofting. Although we do not have firestorm development in any of our cases, we do see a clear threshold above which smoke lofting significantly decreases. With the increase in fire power, however, that pivot point weakens (Figure 12c.) and the relationship between horizontal wind speeds and % smoke above the tropopause becomes more linear.

Of note are the very high maximum wind speeds depicted here. These velocities fall within the hundreds of m s⁻¹ that are expected after a nuclear detonation (Eden, 2004). These very fast winds are ephemeral in nature, occurring directly above the fire area in the lowest level of grid cells. The majority of all vertical velocities above the fire area are much slower. The distribution of winds above 20 m s⁻¹ is shown in Figure 13. As can be seen, most wind speeds are far slower than the noted maxima in Figure 12. And, as background horizontal wind speeds increase, fewer cells see the more extreme vertical velocities. Although LoWi_2 saw a maximum wind speed of almost 150 m s⁻¹, the median updraft velocity (for cells with $w > 20$ m s⁻¹) is actually only 37 m s⁻¹ in the first 15 min after ignition.

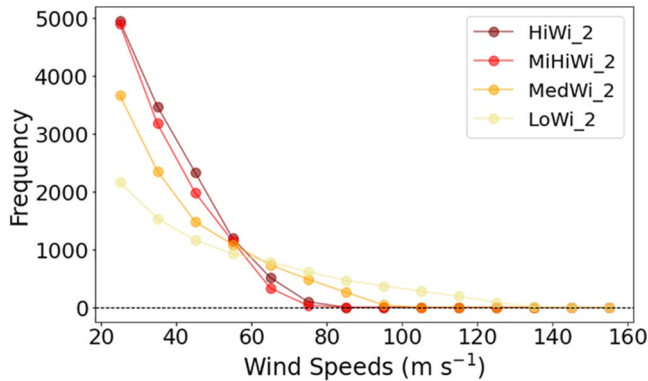


Figure 13. Distribution of vertical velocities greater than 20 m s^{-1} 10 min after ignition for all four 2-km radius wind cases.

Due to computational constraints, we could only assess only four data points for each fire size. Therefore, we recommend further simulations incorporating a larger sample size with more ambient horizontal wind speed variability to better quantify these relationships.

3.3.2. CAPE and Vertical Velocity Relationships With UTLS Smoke

CAPE and vertical velocity (w) in the fire's convection column following ignition can each suggest how much smoke is ultimately lofted into the upper troposphere/lower stratosphere; however, we find that CAPE presents a much stronger signal. For clarification, from here forward, when CAPE is referenced it is shorthand for what Tory et al. (2018) and Tory and Kepert (2021) have defined as fireCAPE, or CAPE specific to parcels of air within the fire plume (after ignition).

CAPE is a measurement of rising potential present in a parcel, based on its buoyancy between the level of free convection (LFC) to the equilibrium level (EL). As such, it is sensitive to background humidity, and is commonly used as an index for deep, moist convection. A number of studies have explored the use of CAPE as a metric for defining fire behavior (Bakhshaii et al., 2020; Potter, 2005; Tory & Thurston, 2015; Tory & Kepert, 2021). Overall, they have found that fires have the potential to greatly increase CAPE, and this modification of the environmental profile can facilitate the development of pyroCb.

The equation for CAPE is found in Equation 3.

$$CAPE = g \int_{LFC}^{EL} \frac{T_{v,p} - T_{v,e}}{T_{v,e}} \partial z. \quad (3)$$

As CAPE is an indicator of potential buoyancy, larger CAPE values indicate a stronger upward acceleration if the parcel does achieve buoyancy. By contrast, vertical velocity specifies the speed at which a parcel is already (currently) ascending or descending. For each simulation, we have calculated the maximum Surface-Based CAPE (SBCAPE, although we will refer to this value simply as CAPE throughout the remainder of the text) following ignition among the air columns above the fire area. We have also calculated maximum vertical velocity in the domain. By comparing these values against the percent of smoke lofted into the upper troposphere (but not against each other), a relationship between smoke rise and each of these metrics emerges. Just as in the discussion on vertical velocities in Section 3.3.1, the CAPE values shown here are local maxima, and not averages across the domain or even above the fire area itself.

CAPE has been selected as a parameter meant to address the influence of water vapor and humidity on smoke lofting potential, as it is largely regarded as a metric for buoyancy potential in a moist column of air. It is used in meteorology for assessing thunderstorm and, most recently, pyroconvection potential (Bakhshaii et al., 2020; Stull, 2015; Peterson, Fromm, et al., 2016), but has been acknowledged to lack precision and, in some cases, reliability due to the assumptions that go into its calculation and its lack of consideration of the fact that storms must first need a convective trigger for CAPE to even matter. Without convection, no storm will develop (Stull, 2015). However, in our cases, there is a certain convective trigger (fire ignition), and parcel theory, upon which CAPE relies, is more likely to hold. The latter is due to the massive radius of our convective area; parcels nearer to the ignition center are shielded from environmental effects such as entrainment for a large part of their ascent. And, unlike many other metrics (e.g., air speeds), CAPE provides insight to how much energy is available to a parcel to work against environmental damping, as opposed to how the parcel is behaving at any one moment in time. This energy is heavily reliant on moisture, which is why CAPE is presented in this study as a proxy for atmospheric humidity.

For the smaller fires, as maximum CAPE of any parcel at the surface and maximum w during the simulation increase, the total smoke injected in the upper troposphere generally increases as well (Figure 14). CAPE has a relatively strong correlation with the percent of smoke that reaches the upper troposphere (R^2 value of 0.82), while vertical velocity has a weaker relationship (R^2 of 0.6). With the increased fire size and higher HRR, the CAPE-smoke relationship weakens slightly (R^2 of 0.77), and the w -smoke relationship deteriorates altogether.

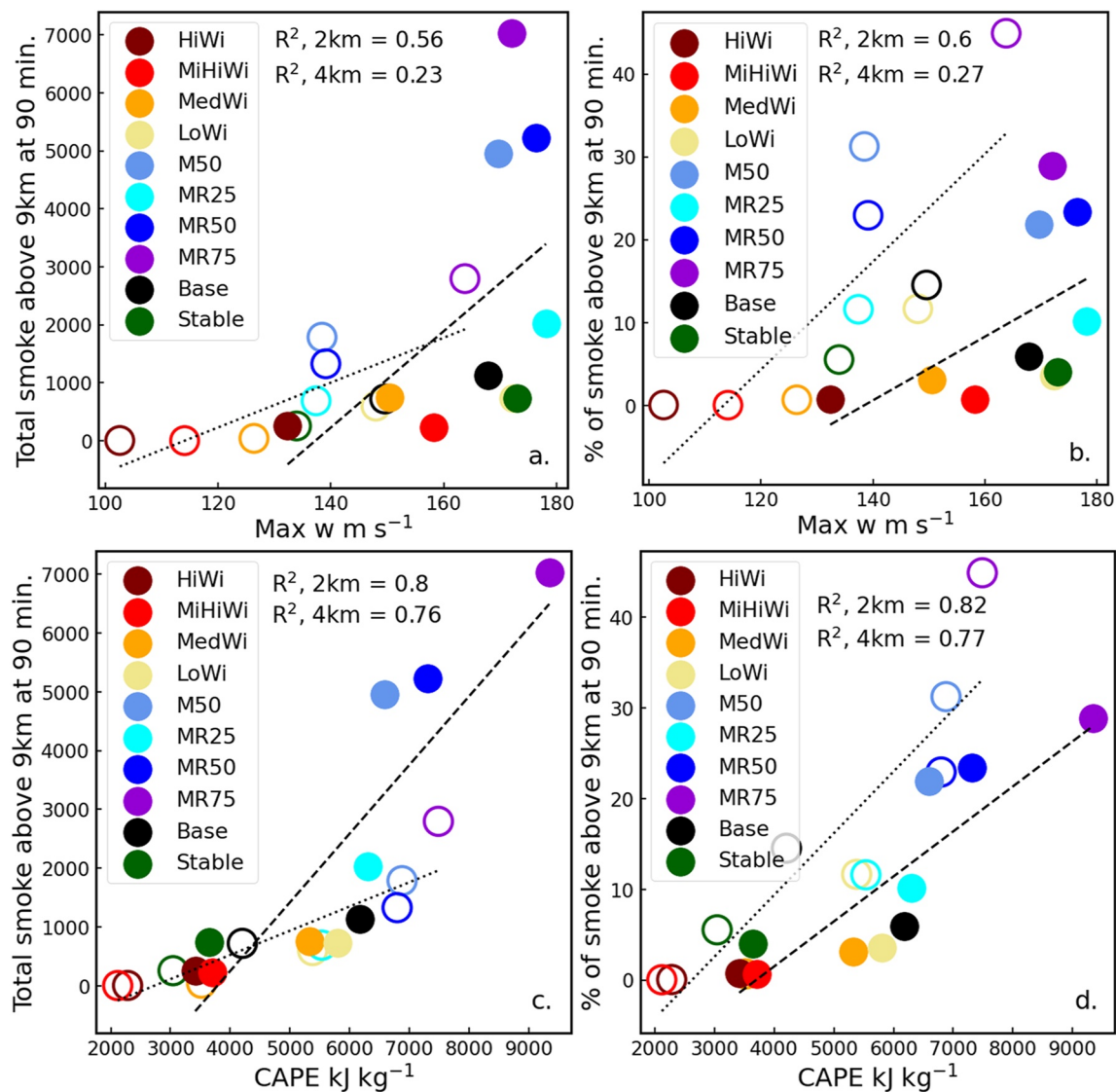


Figure 14. Maximum vertical velocity (a) and (b) and maximum CAPE within the fire area (c) and (d) compared with % smoke rise above 9 km (a) and (c) and total smoke rise above 9 km in Mg (b) and (d), for all 20 simulations. The unfilled markers indicate values from the 2-km radius ignition, while the solid markers correspond to the 4-km radius fire. Each plot has regressions plotted over their 2-km (dotted) and 4-km (dashed) subsets of data points.

As is seen in Figures 14a and 14b, the cases with background relative humidity at 50% or greater stand out against what could otherwise be a strong positive relationship between vertical velocity and smoke lofting: higher w would be linearly correlated with increased smoke rise. The addition of moisture, however, enhances lofting beyond what would be expected via a linear correlation with wind speeds, and the three higher-moisture cases for each fire size inject more smoke higher in the UTLS than what would be otherwise be indicated.

If we consider maximum w as a metric linking smoke lofting with background horizontal winds (as that relationship has already been demonstrated), and CAPE as a metric linking lofting with atmospheric humidity, the insensitivity of the CAPE-smoke relationship to varied wind speeds, when compared with the sensitivity of the w -smoke relationship to moisture, calls attention to how moisture exerts more influence over plume rise than horizontal winds in this study. Of course, in real-case scenarios with variable moisture and wind speeds throughout the vertical extent of the upper troposphere/lower stratosphere, this relationship may become more complex.

Additionally, the cases with specified background moisture in general develop higher CAPE than the dry cases of the same ignition area. However, the dry, quiescent simulations have the highest maximum w values. Although

vertical velocities may reach larger values—particularly in situations where horizontal wind speeds are weak—the role of latent heat release and the generation of buoyancy throughout the vertical extent of the domain plays a more dominant role in plume rise than horizontal winds.

These two findings, therefore, highlight the pivotal role moisture has in dictating plume height. We can conclude that moisture effects are more influential on plume rise than winds.

4. Discussion

In this study, we have evaluated how local meteorology impacts the depth and magnitude of smoke injection in the atmosphere as the result of a large, areal fire ignition. Specifically, the effects of varying background wind speeds, background relative humidity, and atmospheric stability have been examined in a series of LESs considering two different initial fire areas. Additionally, for the cases with moisture, the effects of a radiation parameterization have also been evaluated. Our simulations all employed a homogeneous wildland fuel bed of about 1.3 g cm^{-2} . Previous studies (Penner et al., 1986) have found that plume rise is very sensitive to the fuel burned (and, therefore, the amount of energy released), but we have emphasized the role of the atmosphere and so changes in fuel loading have not been considered here.

Overall, our results all support the conclusions of most previous studies focused on urban fires following a nuclear conflict. Crutzen and Birks (1982), Penner et al. (1986), and Rodden et al. (1965) determined that a moist atmosphere and denser fuels enhance lofting, while a stable atmosphere and increased horizontal wind speeds dampen it. In this study, we find that the inclusion of moisture has the most significant impact—more so than either of the other factors assessed—on deep convection, for both fire sizes. A reduction in horizontal wind speeds also enhances plume rise, while the addition of thermal stability in the ABL dampens it.

We have also shown that an increase in fire size does not increase the overall area average heat release rate; it does, however, escalate the overall energy release from the fuel bed upon ignition, as a larger area is consumed by fire. This stronger radiant flux generates overall stronger convection, but it is spread over a wider swath of land. As a result, with the larger fire area, the gains in smoke lofting compared with the increase in smoke generation are smaller, so many of the 4-km simulations actually exhibit a decrease in the fraction of smoke injected into the UTLS.

Additionally, as convection strengthens (as with the larger fires), factors that directly impact upward motion, thus stifling lofting, become less crucial in influencing injection height. Specifically, horizontal wind speeds begin to lose their dampening strength; stronger upward motion overpowers this element, and for winds greater than or equal to 5 m s^{-1} , a greater percentage of smoke reaches deeper into the UTLS. And, because the convection column lifts smoke so high and so quickly, the effects of radiation on latent heating are also diminished. Overall, UTLS injections for these larger fire simulations begin to trend toward being more comparable with one another. With respect to variations in water vapor, the increased convection has little impact. The influence a moist atmosphere has on smoke rise is derived from energy release into the convection column as water within a rising parcel condenses. Therefore, increased upward motion does not strongly affect the relevance of moisture; in fact, for M50_4 and MR75_4, the height above which half of the smoke is lofted decreases. These differences (or lack thereof) are depicted in Figure 15, where a metric for lofting (the height above which 50% of smoke is lifted) is plotted for each case and fire size.

We compare our final vertical smoke profiles with those of Penner et al. (1986) and Reisner et al. (2018) in Figure 16. We have also run an additional WRF simulation, using the 2-km radius ignition, heavy logging slash, and the input potential temperature, wind, and humidity profiles Reisner et al. (2018) employed in their FIRETEC simulation, for comparison, labeled as Reisner et al. WRF. Unlike the Penner et al. (1986) study, we do not have a specified, constant heat release in our fire area, as shown in Figure 4. Penner et al. (1986) applied heat release rates of 89 kW m^{-2} (10 g cm^{-2} fuel loading), 14 kW m^{-2} (3 g cm^{-2} fuel loading), and 2.2 kW m^{-2} (0.5 g cm^{-2} fuel loading) to simulate three separate fires, with the highest mass loading fire burning for 6 hr, and the other two burning for 12 hr. In contrast, our fires burn for a shorter period of time (1.5 hr) and the surface heat release decreases with time as the fuel in the initial ignition area (mass loading of 1.3 g cm^{-2}) is consumed and the fires begin to spread as perimeter fires. The FIRETEC simulation conducted by Reisner et al. (2018) is more comparable in that regard, as that simulation was run for 40 min, and the heat release replicated what would be

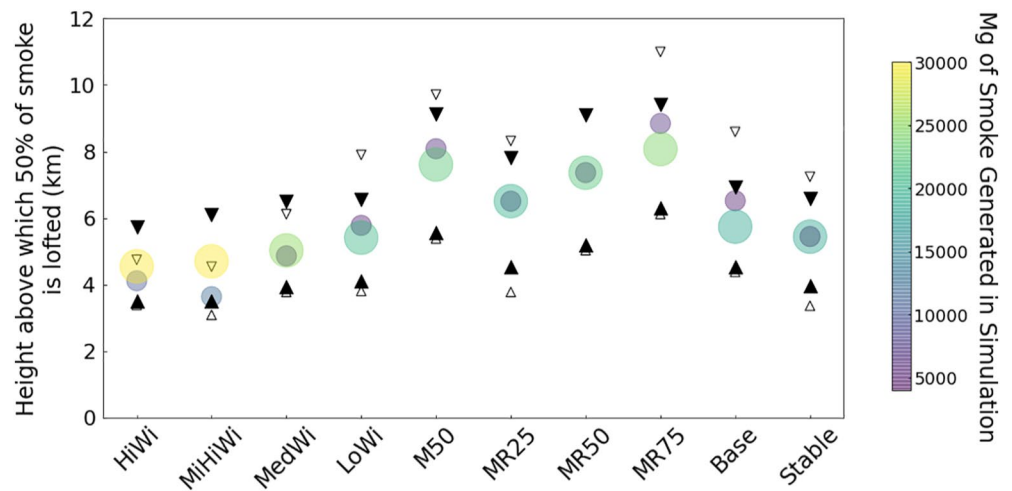


Figure 15. Height above which half of the smoke is lofted, based on the final vertical profiles, for each simulation (circles). Smaller markers indicate the 2-km radius fire; larger markers indicate the 4-km radius fire. Markers are colored according to the amount of smoke generated by that simulation. Additionally, the heights above which 25% and 75% of the smoke is lofted are indicated by triangles (upward facing for 25%, downward for 75%), with smaller, hollow markers signifying the 2-km radius ignition, and larger, filled markers signifying the 4-km radius ignition.

expected with fuel depletion over time. The speed of fuel consumption in both the WRF and FIRETEC simulations may not accurately represent the longevity of urban fires following a nuclear explosion. For comparison, the September 11, 2001 collapse of the World Trade Center ignited a fire within the remains of the complex that burned for 3 days after the attack, at temperatures up to 1000 °C, which were finally weakened by rain in the area on September 14 (Stenchikov et al., 2006).

Interestingly, we find that the distribution of our vertical profiles more closely aligns with those of Penner et al. (1986) than of Reisner et al. (2018). MedWi_2 injects the majority of its smoke between 3 and 5 km, which is akin to Penner et al. (1986)'s 14 kW m⁻² case. MR75_2 has the largest smoke injection at 9 km, slightly below Penner et al. (1986)'s 89 kW m⁻² injection point that peaks just below 11 km. Reisner et al. (2018), on the contrary, saw diminishing smoke with altitude, with the bulk of smoke injection occurring within the lowest kilometer of the model. We suspect this difference results from two factors. First, the Reisner et al. (2018) simulation's lack of a higher smoke concentration in the mid-troposphere indicates the inability of convection from the fire to

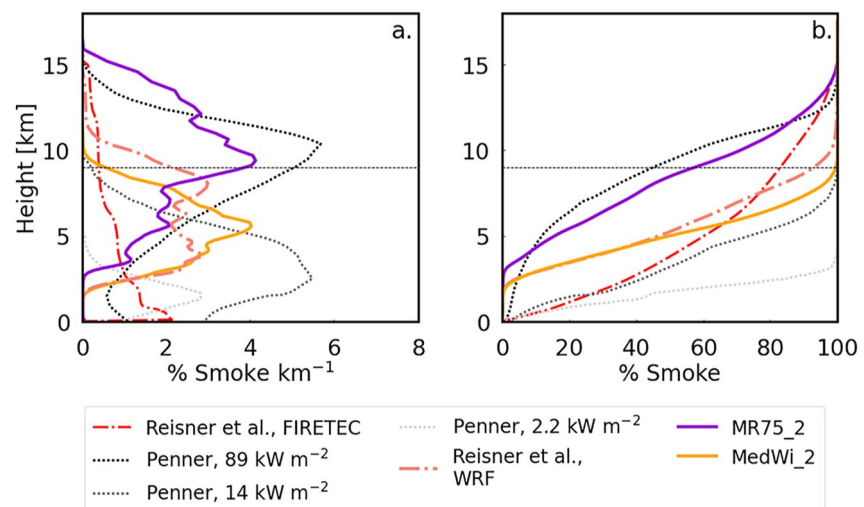


Figure 16. Final vertical smoke distributions of fires simulated in Penner et al. (1986) (dotted), Reisner et al. (2018) (dash-dotted), and this study (MR75_2 and MedWi_2 only, solid). 9 km height is marked by the horizontal dashed line.

overcome the specified stratification throughout the ABL and troposphere. It is likely that this is due both to the lack of latent heating and the light fuel load. Second, the simulations presented in the present study applied an areal ignition of a continuous fuel bed, which enabled a very powerful initial heat release (as evidenced by the maximum CAPE values and vertical velocities previously shown). Although the fuel loading is much lower than that of urban targets, this feature allows the fires to have an initial power release akin to what may be seen with denser, urban fuel beds. This difference between the Reisner et al. (2018) method and the one in this study is also highlighted in a comparison of the WRF simulation using the Reisner et al. (2018) atmospheric profile and the FIRETEC simulation.

Compared with Reisner et al. (2018), our results imply a much different risk factor associated with a nuclear conflict. While our fuel loading is smaller than that of urban targets, and while we did not inform a GCM simulation with the output of our microscale modeling to evaluate the large-scale climate forcing from our fires, we can qualitatively conclude that higher initial relative humidity and more quiescent conditions at the detonation site, as well as a denser fuel load (associated with a higher heat release rate), would ultimately deliver a higher nuclear winter risk than what was suggested by Reisner et al. (2018).

As previously mentioned, the findings in this study are constrained by certain aspects of the model used and the environment selected. Our fuel bed is representative of a wildland source, which has lower fuel density and higher moisture content than urban fuels. The most likely scenario resulting in the ignition of a large, areal fire, as is simulated here, would be the detonation of a powerful weapon, likely in an urban center. WRF-Fire does not currently incorporate cloud seeding, scavenging, or rainout of particulate matter; however, scavenging and rainout are both indirectly captured by the nature of the passive tracer and its parcel-following character. Radiative self-lofting of smoke is not considered. There are no breaks in the fuel bed, nor is there any heterogeneity, as would be found in an urban (or even a mixed wildland) domain. Branding is not considered; lightning is also not modeled. Finally, there is no oxygen starvation within the model, although we demonstrate that oxygen starvation likely does not play a role in our simulations.

This study has examined the influence of several local atmospheric factors on plume rise following the ignition of a large, areal, wildland fire, and has demonstrated that background winds, background relative humidity, and boundary-layer stability are all important. The motivating context for this idealized sensitivity study is to increase understanding of what local atmospheric factors may prime a region for deep smoke and soot lofting following a nuclear conflict. Therefore, to develop a better understanding of how denser fuel sources may influence smoke lofting, future work with an urban fire model and a global climate model, preferably one considering chemistry and aerosol effects, is recommended.

Acknowledgments

Funding for this study has been provided by the Open Philanthropy Project. This work was authored [in part] by the National Renewable Energy Laboratory, operated by Alliance for Sustainable Energy, LLC, for the U.S. Department of Energy (DOE) under Contract DE-AC36-08GO28308. Funding provided by the U.S. Department of Energy Office of Energy Efficiency and Renewable Energy Wind Energy Technologies Office. The views expressed in the article do not necessarily represent the views of the DOE or the U.S. Government. The U.S. Government retains and the publisher, by accepting the article for publication, acknowledges that the U.S. Government retains a nonexclusive, paid-up, irrevocable, worldwide license to publish or reproduce the published form of this work, or allow others to do so, for U.S. Government purposes. This work utilized resources from the University of Colorado Boulder Research Computing Group, which is supported by the National Science Foundation (awards ACI-1532235 and ACI-1532236), the University of Colorado Boulder, and Colorado State University.

Data Availability Statement

The open-source Weather Research and Forecasting (WRF) 4.0.1 model source code can be downloaded at <https://doi.org/10.5065/D6MK6B4K> (Skamarock et al., 2019).

References

- Anderson, H. E. (1982). In *Aids to determining fuel models for estimating fire behavior*. U.S. Department of Agriculture, Forest Service, Intermountain Forest and Range Experiment Station. Tech. Rep. No. INT-GTR-122. <https://doi.org/10.2737/INT-GTR-122>
- Arms Control Association. (2019). *Nuclear weapons: Who has what at a glance*.
- Baek, S. (2017). A revised radiation package of G-packed McICA and two-stream approximation: Performance evaluation in a global weather forecasting model. *Journal of Advances in Modeling Earth Systems*, 9(3), 1628–1640. <https://doi.org/10.1002/2017MS000994>
- Bakhshaii, A., Johnson, E. A., & Nayebi, K. (2020). Wildfire pyroconvection and CAPE: Buoyancy's drying and atmospheric intensification—Fort McMurray. *Atmosphere Multidisciplinary Digital Publishing Institute*, 11(7), 763. <https://doi.org/10.3390/atmos11070763>
- Barbero, R., Abatzoglou, J. T., Larkin, N. K., Kolden, C. A., & Stocks, B. (2015). Climate change presents increased potential for very large fires in the contiguous United States. *International Journal of Wildland Fire*, 24(7), 892–899. <https://doi.org/10.1071/WF15083>
- Boer, M. M., Resco de Dios, V., & Bradstock, R. A. (2020). Unprecedented burn area of Australian mega forest fires. *Nature Climate Change*. *Nature Publishing Group*, 10(3), 171–172. <https://doi.org/10.1038/s41558-020-0716-1>
- Clark, T. L., Coen, J., & Latham, D. (2004). Description of a coupled atmosphere - Fire model. *International Journal of Wildland Fire*, 13(1), 49. <https://doi.org/10.1071/WF03043>
- Coen, J. L., Cameron, M., Michalakes, J., Patton, E. G., Riggan, P. J., & Yedinak, K. M. (2013). WRF-Fire: Coupled weather-wildland fire modeling with the weather research and forecasting model. *Journal of Applied Meteorology and Climatology*, 52(1), 16–38. <https://doi.org/10.1175/JAMC-D-12-023.1>
- Cotton, W. R. (1985). Atmospheric convection and nuclear winter: A new simulation of a large urban firestorm shows how smoke and soot might enter the stratosphere and alter the earth's climate. *American Scientist*, 73(3), 275–280. https://doi.org/10.1007/978-1-4899-7164-7_36

- Countryman, C. M. (1964). *Mass fires and fire behavior (Tech. Rep. No. RS-RP-19)*. Pacific Southwest Forest and Range Experiment Station, Forest Service, US Department of Agriculture.
- Coupe, J., Bardeen, C. G., Robock, A., & Toon, O. B. (2019). Nuclear winter responses to nuclear war between the United States and Russia in the Whole Atmosphere Community Climate Model Version 4 and the Goddard Institute for Space Studies ModelE. *Journal of Geophysical Research: Atmosphere*, *124*(15). <https://doi.org/10.1029/2019JD030509>
- Covey, C., Schneider, S. H., & Thompson, S. L. (1984). Global atmospheric effects of massive smoke injections from a nuclear war: Results from general circulation model simulations. *Nature*, *308*(5954), 21–25. <https://doi.org/10.1038/308021a0>
- Crutzen, P. J., & Birks, J. W. (1982). The atmosphere after a nuclear war: Twilight at noon. *Ambio*, *11*(2/3), 114–125.
- Eden, L. (2004). *Whole world on fire: Organizations, knowledge, and nuclear weapons devastation*. Cornell University Press.
- Freitas, S. R., Longo, K. M., Trentmann, J., & Latham, D. (2010). Technical Note: Sensitivity of 1-D smoke plume rise models to the inclusion of environmental wind drag. *Atmospheric Chemistry and Physics*, *10*. <https://doi.org/10.5194/acp-10-585-2010>
- Fritsch, J. M., & Chappell, C. F. (1980). Numerical Prediction of Convectively Driven Mesoscale Pressure Systems. Part I: Convective Parameterization. *Journal of the Atmospheric Sciences*, *37*, 1722–2173. [https://doi.org/10.1175/1520-0469\(1980\)037<1722:npocdm>2.0.co;2](https://doi.org/10.1175/1520-0469(1980)037<1722:npocdm>2.0.co;2)
- Fromm, M., Lindsey, D. T., Servranckx, R., Yue, G., Trickl, T., Sica, R., & Godin-Beekmann, S. (2010). The untold story of Pyrocumulonimbus. *Bulletin of the American Meteorological Society*, *91*(9), 1193–1210. <https://doi.org/10.1175/2010BAMS3004.1>
- Ghan, S. J., MacCracken, M. C., & Walton, J. J. (1988). Climatic response to large atmospheric smoke injections: Sensitivity studies with a tropospheric general circulation model. *Journal of Geophysical Research*, *93*(D7), 8315–8337. <https://doi.org/10.1029/jd093id07p08315>
- Gillett, N. P., Weaver, A. J., Zwiers, F. W., & Flannigan, M. D. (2004). Detecting the effect of climate change on Canadian forest fires. *Geophysical Research Letters*, *31*(18). <https://doi.org/10.1029/2004gl020876>
- Glasstone, S., & Dolan, P. J. (1977). *The effects of nuclear weapons*. Department of Defense. (Google-Books-ID: s4NwjdTWqXMC).
- Goss, M., Swain, D. L., Abatzoglou, J. T., Sarhadi, A., Kolden, C. A., Williams, A. P., & Duffenbaugh, N. S. (2020). Climate change is increasing the likelihood of extreme autumn wildfire conditions across California. *Environmental Research Letters*, *15*(9), 094016. <https://doi.org/10.1088/1748-9326/ab83a7>
- Graf, H.-F., Herzog, M., Oberhuber, J. M., & Textor, C. (1999). Effect of environmental conditions on volcanic plume rise. *Journal of Geophysical Research*, *104*(D20), 24309–24320. <https://doi.org/10.1029/1999JD900498>
- Huggett, C. (1980). Estimation of rate of heat release by means of oxygen consumption measurements. *Fire and Materials*, *4*(2), 61–65. <https://doi.org/10.1002/fam.810040202>
- Jägermeyr, J., Robock, A., Elliott, J., Müller, C., Xia, L., & Khabarov, N. (2020). A regional nuclear conflict would compromise global food security. *Proceedings of the National Academy of Sciences*, *117*(13), 7071–7081. <https://doi.org/10.1073/pnas.1919049117>
- Jiménez, P. A., Muñoz Esparza, D., & Kosović, B. (2018). A high resolution coupled fire–atmosphere forecasting system to minimize the impacts of wildland fires: Applications to the Chimney Tops II wildland event. *Atmosphere*, *9*(5), 197. <https://doi.org/10.3390/atmos9050197>
- Klemp, J. B., Dudhia, J., & Hassiotis, A. D. (2008). An upper gravity-wave absorbing layer for NWP applications. *Monthly Weather Review*, *136*(10), 3987–4004. <https://doi.org/10.1175/2008MWR2596.1>
- Koo, E., Pagni, P. J., Weise, D. R., & Woycheese, J. P. (2010). Firebrands and spotting ignition in large-scale fires. *International Journal of Wildland Fire*, *19*(7), 818–843. CSIRO Publishing. <https://doi.org/10.1071/WF07119>
- Krikken, F., Lehner, F., Haustein, K., Drobyshev, I., & van Oldenborgh, G. J. (2019). Attribution of the role of climate change in the forest fires in Sweden 2018. *Natural Hazards and Earth System Sciences Discussions*, *1–24*. <https://doi.org/10.5194/nhess-2019-206>
- Kristensen, H. M. (2019). Chapter 1 - Global Nuclear Arsenals, 1990–2018. In J. E. Doyle (Ed.), *Nuclear safeguards, security, and nonproliferation* (2nd ed., pp. 3–35). Butterworth-Heinemann. <https://doi.org/10.1016/B978-0-12-803271-8.00001-1>
- Lareau, N. P., & Clements, C. B. (2016). Environmental controls on pyrocumululus and pyrocumulonimbus initiation and development. *Atmospheric Chemistry and Physics*, *16*(6), 4005–4022. <https://doi.org/10.5194/acp-16-4005-2016>
- Luderer, G., Trentmann, J., Winterrath, T., Textor, C., Herzog, M., Graf, H. F., & Andreae, M. O. (2006). Modeling of biomass smoke injection into the lower stratosphere by a large forest fire (Part II): Sensitivity studies. *Atmospheric Chemistry and Physics Discussions*, *6*(4), 6081–6124. European Geosciences Union. <https://doi.org/10.5194/acp-6-5261-2006>
- Mandel, J., Beezley, J. D., & Kochanski, A. K. (2011). Coupled atmosphere-wildland fire modeling with WRF-Fire. *Geoscientific Model Development*, *4*(3), 591–610. arXiv: 1102.1343. <https://doi.org/10.5194/gmd-4-591-2011>
- Mills, M. J., Toon, O. B., Lee-Taylor, J., & Robock, A. (2014). Multidecadal global cooling and unprecedented ozone loss following a regional nuclear conflict. *Earth's Future*, *2*(4), 161–176. <https://doi.org/10.1002/2013ef000205>
- Mills, M. J., Toon, O. B., Turco, R. P., Kinnison, D. E., & Garcia, R. R. (2008). Massive global ozone loss predicted following regional nuclear conflict. *Proceedings of the National Academy of Sciences*, *105*(14), 5307–5312. <https://doi.org/10.1073/pnas.0710058105>
- Moncrieff, M. W., & Miller, M. J. (1976). The dynamics and simulation of tropical cumulonimbus and squall lines. *Quarterly Journal of the Royal Meteorological Society*, *102*(432), 373–394. <https://doi.org/10.1002/qj.49710243208>
- Morton, B. R. (1964). Fire and wind. *Science Progress*, *52*(206), 249–258.
- Muñoz Esparza, D., Kosović, B., Jiménez, P. A., & Coen, J. L. (2018). An accurate fire-spread algorithm in the weather research and forecasting model using the level-set method. *Journal of Advances in Modeling Earth Systems*, *10*(4), 908–926. <https://doi.org/10.1002/2017MS001108>
- Muñoz-Esparza, D., & Kosović, B. (2018). Generation of inflow turbulence in large-eddy simulations of nonneutral atmospheric boundary layers with the cell perturbation method. *Monthly Weather Review*, *146*(6), 1889–1909. <https://doi.org/10.1175/MWR-D-18-0077.1>
- Nakanishi, M., & Niino, H. (2009). Development of an improved turbulence closure model for the atmospheric boundary layer. *Journal of the Meteorological Society of Japan*, *87*(5), 895–912. <https://doi.org/10.2151/jmsj.87.895>
- Osher, S., & Sethian, J. A. (1988). Fronts propagating with curvature-dependent speed: Algorithms based on Hamilton-Jacobi formulations. *Journal of Computational Physics*, *79*(1), 12–49. [https://doi.org/10.1016/0021-9991\(88\)90002-2](https://doi.org/10.1016/0021-9991(88)90002-2)
- Patton, E. G., & Coen, J. L. (2004). *WRF-Fire: A coupled atmosphere-fire module for WRF* (Vol. 3).
- Penner, J. E., Haselman, L. C., & Edwards, L. L. (1986). Smoke-plume distributions above large-scale fires: Implications for simulations of nuclear winter. *Journal of Climate and Applied Meteorology*, *25*(10), 1434–2144. [https://doi.org/10.1175/1520-0450\(1986\)025<1434:spdals>2.0.co;2](https://doi.org/10.1175/1520-0450(1986)025<1434:spdals>2.0.co;2)
- Peterson, D. A., Campbell, J. R., Hyer, E. J., Fromm, M. D., Kablick, G. P., Cossuth, J. H., & DeLand, M. T. (2018). Wildfire-driven thunderstorms cause a volcano-like stratospheric injection of smoke. *NPJ Climate and Atmospheric Science*, *1*(1). <https://doi.org/10.1038/s41612-018-0039-3>
- Peterson, D. A., Fromm, M. D., Solbrig, J. E., Hyer, E. J., Surratt, M. L., & Campbell, J. R. (2016). Detection and inventory of intense pyroconvection in Western North America using GOES-15 daytime infrared data. *Journal of Applied Meteorology and Climatology*, *56*(2), 471–493. <https://doi.org/10.1175/JAMC-D-16-0226>
- Peterson, D. A., Hyer, E. J., Campbell, J. R., Solbrig, J. E., & Fromm, M. D. (2016). A conceptual model for development of intense pyrocumulonimbus in Western North America. *Monthly Weather Review*, *145*(6), 2235–2255. <https://doi.org/10.1175/MWR-D-16-0232.1>

- Peterson, D. A., Hyer, E. J., & Wang, J. (2014). Quantifying the potential for high-altitude smoke injection in the North American boreal forest using the standard MODIS fire products and subpixel-based methods. *Journal of Geophysical Research: Atmosphere*, *119*(6), 3401–3419. <https://doi.org/10.1002/2013JD021067>
- Potter, B. E. (2005). The role of released moisture in the atmospheric dynamics associated with wildland fires. *International Journal of Wildland Fire*, *14*(1), 77. <https://doi.org/10.1071/wf04045>
- Powers, J. G., Klemp, J. B., Skamarock, W. C., Davis, C. A., Dudhia, J., Gill, D. O., & Duda, M. G. (2017). The weather research and forecasting model: Overview, system efforts, and future directions. *Bulletin of the American Meteorological Society*, *98*(8), 1717–1737. <https://doi.org/10.1175/BAMS-D-15-00308.1>
- Reisner, J., D'Angelo, G., Koo, E., Even, W., Hecht, M., Hunke, E., & Cooley, J. (2018). Climate impact of a regional nuclear weapons exchange: An improved assessment based on detailed source calculations. *Journal of Geophysical Research: Atmosphere*, *123*(5), 2752–2772. <https://doi.org/10.1002/2017JD027331>
- Robock, A., Oman, L., & Stenchikov, G. L. (2007). Nuclear winter revisited with a modern climate model and current nuclear arsenals: Still catastrophic consequences. *Journal of Geophysical Research: Atmosphere*, *112*(D13). <https://doi.org/10.1029/2006JD008235>
- Robock, A., Oman, L., Stenchikov, G. L., Toon, O. B., Bardeen, C., & Turco, R. P. (2007). Climatic consequences of regional nuclear conflicts. *Atmospheric Chemistry and Physics*, *65*. <https://doi.org/10.5194/acp-7-2003-2007>
- Robock, A., & Toon, O. B. (2012). Self-assured destruction: The climate impacts of nuclear war. *Bulletin of the Atomic Scientists*, *68*(5), 66–74. <https://doi.org/10.1177/0096340212459127>
- Robock, A., Toon, O. B., & Bardeen, C. G. (2019). Comment on Climate Impact of a Regional Nuclear Weapon Exchange: An Improved Assessment Based on Detailed Source Calculations by Reisner et al. *Journal of Geophysical Research: Atmosphere*, *124*(23), 12953–12958. <https://doi.org/10.1029/2019JD030777>
- Robock, A., Toon, O. B., Bardeen, C. G., Xia, L., Kristensen, H. M., McKinzie, M., & Turco, R. P. (2019). How an India-Pakistan nuclear war could start and have global consequences. *Bulletin of the Atomic Scientists*, *75*(6), 273–279. <https://doi.org/10.1080/00963402.2019.1680049>
- Rodden, R. M., John, F. I., & Laurino, R. (1965). *Exploratory Analysis of fire storms (Tech. Rep.)*. Stanford Research Inst MENLO PARK CA. SIPRI. (2019). *World nuclear forces*. Retrieved from <https://sipri.org/yearbook/2019/06/>
- Skamarock, W. C., Klemp, J. B., Dudhia, J., Gill, D. O., Liu, Z., & Berner, J. (2019). *A Description of the Advanced Research Wrf Model Version 4* (Vol. 145). National Center for Atmospheric Research.
- Small, R. D., & Heikes, K. E. (1988). Early cloud formation by large area fires. *Journal of Applied Meteorology*, *27*(5), 6542–6663. [https://doi.org/10.1175/1520-0450\(1988\)027<0654:ecfbla>2.0.co;2](https://doi.org/10.1175/1520-0450(1988)027<0654:ecfbla>2.0.co;2)
- Sofiev, M., Ermakova, T., & Vankevich, R. (2012). February). Evaluation of the smoke-injection height from wild-land fires using remote-sensing data. *Atmospheric Chemistry and Physics*, *12*(4), 1995–2006. <https://doi.org/10.5194/acp-12-1995-2012>
- Stenchikov, G., Lahoti, N., Diner, D. J., Kahn, R., Lioy, P. J., & Georgopoulos, P. G. (2006). Multiscale plume transport from the collapse of the world trade center on september 11, 2001. *Environmental Fluid Mechanics*, *6*(5), 425–450. <https://doi.org/10.1007/s10652-006-9001-8>
- Stull, R. B. (2015). *Practical meteorology: An algebra-based survey of atmospheric science*.
- Tarifa, C. S., Notario, P. P. d., & Moreno, F. G. (1965). On the flight paths and lifetimes of burning particles of wood. *Symposium (International) on Combustion*, *10*(1), 1021–1037. [https://doi.org/10.1016/S0082-0784\(65\)80244-2](https://doi.org/10.1016/S0082-0784(65)80244-2)
- Thompson, G., Field, P. R., Rasmussen, R. M., & Hall, W. D. (2008). Explicit forecasts of winter precipitation using an improved bulk microphysics scheme. Part II: Implementation of a new snow parameterization
- Thompson, G., Rasmussen, R. M., & Manning, K. (2004). Explicit forecasts of winter precipitation using an improved bulk microphysics scheme. Part I: Description and sensitivity analysis. *Monthly Weather Review*, *132*(2), 5192–5542. [https://doi.org/10.1175/1520-0493\(2004\)132<0519:efowpu>2.0.co;2](https://doi.org/10.1175/1520-0493(2004)132<0519:efowpu>2.0.co;2)
- Thornton, W. (1917). Xv. the relation of oxygen to the heat of combustion of organic compounds. *The London, Edinburgh, and Dublin Philosophical Magazine and Journal of Science*, *33*(194), 196–203. <https://doi.org/10.1080/14786440208635627>
- Toon, O. B., Bardeen, C. G., Robock, A., Xia, L., Kristensen, H., McKinzie, M., & Turco, R. P. (2019). Rapidly expanding nuclear arsenals in Pakistan and India portend regional and global catastrophe. *Science Advances*, *5*(10), eaay5478. <https://doi.org/10.1126/sciadv.aay5478>
- Toon, O. B., Robock, A., & Turco, R. P. (2008). Environmental consequences of nuclear war. *Physics Today*, *61*(12), 37–42. <https://doi.org/10.1063/1.3047679>
- Toon, O. B., Robock, A., Turco, R. P., Bardeen, C., Oman, L., & Stenchikov, G. L. (2007). Consequences of regional-scale nuclear conflicts. *Science*, *315*(5816), 1224–1225. <https://doi.org/10.1126/science.1137747>
- Tory, K., & Thurston, W. (2015). *Pyrocumulonimbus: A literature review*. Bushfire and Natural Hazards CRC.
- Tory, K. J., & Kepert, J. D. (2021). Pyrocumulonimbus firepower threshold: Assessing the Atmospheric Potential for pyroCb. *Weather and Forecasting*, *36*(2), 439–456. <https://doi.org/10.1175/waf-d-20-0027.1>
- Tory, K. J., Thurston, W., & Kepert, J. D. (2018). Thermodynamics of pyrocumululus: A conceptual study. *Monthly Weather Review*, *146*(8), 2579–2598. <https://doi.org/10.1175/mwr-d-17-0377.1>
- Trentmann, J., Luderer, G., Winterrath, T., Fromm, M. D., Servranckx, R., Textor, C., & Andreae, M. O. (2006). Modeling of biomass smoke injection into the lower stratosphere by a large forest fire (Part I): Reference simulation. *Atmospheric Chemistry and Physics Discussions*, *6*(4), 6041–6080. <https://doi.org/10.5194/acp-6-5247-2006>
- Turco, R. P., Toon, O. B., Ackerman, T. P., Pollack, J. B., & Sagan, C. (1983). Nuclear winter: Global consequences of multiple nuclear explosions. *Science*, *222*(4630), 1283–1292. <https://doi.org/10.1126/science.222.4630.1283>
- Turco, R. P., Toon, O. B., Ackerman, T. P., Pollack, J. B., & Sagan, C. (1990). Climate and smoke: An appraisal of nuclear winter. *Science*, *247*(4939), 166–176. <https://doi.org/10.1126/science.11538069>
- Wagman, B. M., Lundquist, K. A., Tang, Q., Glascoe, L. G., & Bader, D. C. (2020). Examining the climate effects of a regional nuclear weapons exchange using a multiscale atmospheric modeling approach. *Journal of Geophysical Research: Atmosphere*, *125*(24), e2020JD033056. <https://doi.org/10.1029/2020jd033056>
- Wellerstein, A. (2012). *Nukemap*. Retrieved from <https://nuclearsecrecy.com/nukemap/>
- Westerling, A. L., Bryant, B. P., Preisler, H. K., Holmes, T. P., Hidalgo, H. G., Das, T., & Shrestha, S. R. (2011). Climate change and growth scenarios for California wildfire. *Climatic Change*, *109*(1), 445–463. <https://doi.org/10.1007/s10584-011-0329-910.1007/s10584-011-0329-9>
- Wilcox, L. J., Hoskins, B. J., & Shine, K. P. (2012). A global blended tropopause based on ERA data. Part I: Climatology. *Quarterly Journal of the Royal Meteorological Society*, *138*(664), 561–575. <https://doi.org/10.1002/qj.951>
- Xia, L., Robock, A., Mills, M., Stenke, A., & Helfand, I. (2015). Decadal reduction of Chinese agriculture after a regional nuclear war. *Earth's Future*, *3*(2), 37–48. <https://doi.org/10.1002/2014ef000283>
- Yu, P., Toon, O. B., Bardeen, C. G., Zhu, Y., Rosenlof, K. H., Portmann, R. W., & Robock, A. (2019). Black carbon lofts wildfire smoke high into the stratosphere to form a persistent plume. *Science*, *365*(6453), 587–590. <https://doi.org/10.1126/science.aax1748>